Viscous and hyperviscous filtering for direct and large-eddy simulation

Eric Lamballais, Rodrigo Vicente Cruz, Rodolphe Perrin

Version of Record: https://www.sciencedirect.com/science/article/pii/S0021999121000073
Manuscript_95117f5520e24e7b21edb2664378d3bc

Viscous and hyperviscous filtering for direct and large-eddy simulation

Eric Lamballais[a], Rodrigo Vicente Cruz[a], Rodolphe Perrin[b]

[a] *Incompressible Turbulence and Control Group, Pprime Institute, CNRS - Univ-Poitiers - ENSMA, France*
[b] *Department of Mechanical Engineering, Faculty of Engineering, Kasetsart University Sriracha, Thailand*

Abstract

This work is dedicated to the solution filtering technique for performing direct and large-eddy simulation. It is shown that this approach is equivalent to the use of spectral viscosity as a possible ersatz of subgrid-scale modelling. In the framework of finite-difference schemes, the filter operator can be designed to ensure time consistency while easily controlling the level and scale selectivity of the dissipation thus introduced. Then, a new family of filter schemes is developed in order to represent both the molecular and artificial dissipations. The resulting viscous filter operator is straightforward to implement through a simple modification of its coefficients that depend on the molecular/artificial viscosity and the time step. A definitive advantage in terms of computational efficiency is obtained for computational configurations where the time step is restricted by the Fourier condition, as a simple alternative to implicit time integration of the viscous term. Numerical tests clearly show that this viscous filtering method is flexible, accurate and numerically stable at large Fourier number.

Keywords: Direct and large-eddy simulation, Solution filtering, Finite-difference schemes, High-order methods, 3D Taylor-Green vortex flow, Turbulent pipe flow.

*Corresponding author.
Email address: eric.lamballais@univ-poitiers.fr (Eric Lamballais)

1. Introduction

In the context of large-eddy simulation (LES), spatial filtering can refer to different concepts and techniques, as a potential source of misunderstanding between users and developers in this field of computational fluid dynamics. The essential meaning of spatial filtering is related to the LES formalism itself as a tool of decomposition between the large-scale component of the solution and its residual small-scale component designated as the subgrid-scale (SGS) part. This first concept has been widely developed with the purpose to derive the governing equations of the large-scale motion while introducing the unknown SGS tensor in the framework of a closure problem. For the general background based on this way to define the LES problem, the reader is referred to the textbooks [1, 2, 3] which also include the presentation of the most popular SGS models. In this study, this primitive meaning of spatial filtering is not addressed. The related SGS modelling is also not considered, avoiding the difficult questions about the way to account for this "implicit filtering" in the SGS model itself. For the most popular SGS model, namely the Smagorinsky model, the spatial filtering, to which the solution is actually subjected, is a model feature. This feature can only be known *a posteriori*, as an output of the LES, with a major role of the numerical error for the filtering actually obtained [4].

In this study, we are interested in the technique that consists in the application of spatial filtering every time step on the solution during the time advancement of the governing equations. This technique is sometimes referred as "solution filtering" [5] or as "relaxation filtering" [6, 7]. It can also be designated as "explicit filtering", but this term is potentially confusing with the SGS modelling approach where the non-linear convective terms, based on the implicitly filtered (i.e. large-scale) solution, are themselves filtered with a given operator to define an alternative SGS tensor in a modified closure problem [8, 9, 10]. Here, for simplicity, the term "solution filtering" is preferred to clearly express that the filter operation is applied directly on the solution without any reference to other formalisms or non-linearity treatments. We also only focus on the systematic application of the filter every time step, even if a periodic application every n time steps can also be an option to control the resulting artificial dissipation while saving computational time [11, 12, 13, 14].

The solution filtering approach is shared by a wide community in the field of LES as well as in direct numerical simulation (DNS), see for instance

[15, 16, 11, 17, 18, 19]. When used in DNS, it can be viewed as a way to control the development of numerical oscillations, due for instance to aliasing errors, when the viscous term is not strong enough to ensure this control [20]. Typically, it enables simulators to perform DNS at marginal resolution while improving the physical realism of their solutions which can be virtually free from small-scale spurious oscillations. When this idea is pushed further using coarse computational mesh at high Reynolds number, the filtering solution strategy is referred as an ersatz of SGS modelling in a fuzzy formalism mainly based on considerations about the expected functional role of the SGS uncaptured by the computational mesh. Viewed in this perspective, this approach may be classified in the field of implicit LES, the solution filtering corresponding to an artificial regularisation process applied throughout the calculation. Since its very beginning through the MILES approach [21], implicit LES has become very popular with the development of a wide range of technics to ensure regularisation (see for instance the collective book [22]). In this work, the goal is not to propose a new approach for implicit LES but to develop a new technique that can be put in this perspective while being firstly useful for DNS.

To introduce artificial dissipation for regularisation purposes, the most popular method is to differentiate the convective term using upwind schemes. An alternative is to boost artificially the viscous term through an overestimation of the second derivatives at small scales, as proposed by [23] where a comparison with the traditional upwind-based strategy is presented for a one-dimensional (1D) linear convection/diffusion equation. In [23], and in a more detailed way in [4], it has been shown that this type of numerical dissipation is the finite-difference counterpart of spectral vanishing viscosity (SVV) [24, 25, 26, 27]. In this paper, also based on a finite-difference framework, the links between SVV, boosted second derivative and filtering are clarified to open the way for a new technique of solution filtering.

The manuscript is organized as follows. In section 2, a generic finite-difference operator is defined with a classic definition of its coefficient relations up to a given order of accuracy. Then, the role of solution filtering is described in section 3 by considering a 1D model equation where the filtering operation can be clearly expressed inside the time advancement. In this simplified framework, an equivalent SVV is introduced in section 4 as a function of the filter transfer function. Based on this equivalence, the strength and the scale-selectivity of the filter can be controlled through the scaling of the scheme coefficients while ensuring the time consistency of the resulting

regularisation operator. This principle is extended in section 5 in order to incorporate the molecular dissipation into the filter scheme. In section 6, the numerical accuracy and stability of this new type of filtering, called "viscous filtering", is analysed through spatial and temporal convergence tests. Then, DNS/LES results are presented in section 7 to assess the viscous filtering strategy in demanding computational configurations involving fully developed turbulence. The major advantage of viscous filtering, in terms of numerical stability, is clearly exhibited, as an efficient alternative strategy to time implicit integration of the viscous term. The main conclusions are summarized in section 8 while drawing perspectives for further developments. Finally, an appendix is provided to clearly establish the close link between viscous filter and second derivative finite-difference schemes.

2. Filtering scheme and transfer function

Here, the filtering approach is considered in the framework of finite-difference schemes. For simplicity, the discretization is based on a regular mesh and the formalism is presented in 1D through the basic filtering operator expressed as

$$\begin{aligned}\alpha_f \hat{f}_{i-1} + \hat{f}_i + \alpha_f \hat{f}_{i+1} = a_f f_i \quad &+ \quad b_f \frac{f_{i-1}+f_{i+1}}{2} + c_f \frac{f_{i-2}+f_{i+2}}{2} \\ &+ \quad d_f \frac{f_{i-3}+f_{i+3}}{2} + e_f \frac{f_{i-4}+f_{i+4}}{2}\end{aligned} \tag{1}$$

with its associated transfer function

$$T(k\Delta x) = \frac{a_f + b_f \cos(k\Delta x) + c_f \cos(2k\Delta x) + d_f \cos(3k\Delta x) + e_f \cos(4k\Delta x)}{1 + 2\alpha_f \cos(k\Delta x)} \tag{2}$$

where $f_i = f(x_i)$ are the values of a generic function $f(x)$ on the nodes $x_i = (i-1)\Delta x$, $\hat{f}_i$ are the filtered values and k is the wavenumber. To provide a low-pass filter, it is common to impose the value of $T(k\Delta x)$ at the cutoff wavenumber $k_c = \pi/\Delta x$ with for instance

$$T(k_c \Delta x) = 1 - \sigma \tag{3}$$

where $0 \leq \sigma \leq 1$. In the context of numerical simulation, the most popular choice is to fully remove the grid-to-grid wavelength using $\sigma = 1$.

In addition to condition (3), Taylor's expansion can provide extra constraints on the set of coefficients $(\alpha_f, a_f, b_f, c_f, d_f, e_f)$ in order to reach a given order of accuracy, with

$$\begin{aligned}
1+2\alpha_f &= a_f + b_f + c_f + d_f + e_f && (\Delta x^2) && (4)\\
2\alpha_f &= b_f + 4c_f + 9d_f + 16e_f && (\Delta x^4) && (5)\\
2\alpha_f &= b_f + 16c_f + 81d_f + 256e_f && (\Delta x^6) && (6)\\
2\alpha_f &= b_f + 64c_f + 729d_f + 4096e_f && (\Delta x^8) && (7)\\
2\alpha_f &= b_f + 256c_f + 6561d_f + 65536e_f && (\Delta x^{10}) && (8)
\end{aligned}$$

For the present 6 coefficient scheme, condition (3) expressed as

$$a_f - b_f + c_f - d_f + e_f = (1-\sigma)(1-2\alpha_f) \tag{9}$$

enables 10^{th}-order accuracy.

If only 6^{th}-order accuracy is desired, an option is to reduce the stencil of (1) by imposing $e_f = 0$ while leaving free α_f, this choice leading to the set of coefficients

$$\begin{aligned}
a_f &= \frac{\sigma(10\alpha - 5) + 16}{16}\\
b_f &= \frac{\sigma(15 - 30\alpha) + 64\alpha}{32}\\
c_f &= \frac{\sigma(-3 + 6\alpha)}{16}\\
d_f &= \frac{\sigma(1 - 2\alpha)}{32}
\end{aligned} \tag{10}$$

in which the very popular scheme of [28] corresponds to the assumption $\sigma = 1$ with $a_f = \dfrac{11+10\alpha}{16}$, $b_f = \dfrac{15+34\alpha}{32}$, $c_f = \dfrac{-3+6\alpha}{16}$ and $d_f = \dfrac{1-2\alpha}{32}$. For the more general scheme given by (10), the two control parameters of the filter behaviour are α and σ. The former defines the scale-selectivity of the filtering whereas the latter specifies its attenuation level through its prescription on the grid-to-grid oscillations. These two features are illustrated in figure 1.

3. Functional role of solution filtering

Despite its name, as already mentioned in the introduction section 1, this type of filtering operator has no direct connection with the filtering

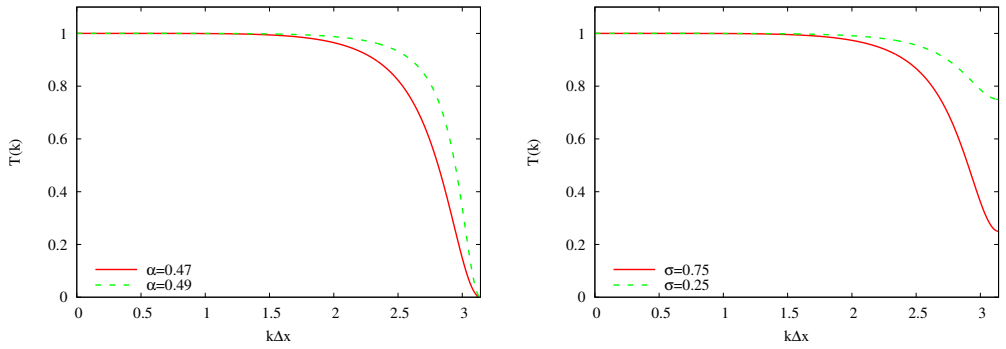

Figure 1: Left: highly ($\alpha = 0.49$) and moderately ($\alpha = 0.47$) scale-selective filtering for $\sigma = 1$. Right: soft ($\sigma = 0.25$) and medium ($\sigma = 0.75$) filtering for $\alpha = 0.47$.

framework of the LES formalism. To make clear this essential point, let us consider

$$\frac{du}{dt} = \lambda u \tag{11}$$

as a simple model equation of the DNS/LES governing equations. The complex variable λ can be defined to consider a generic convection/diffusion equation with $\lambda = -ick - \nu k^2$ where ν is the molecular viscosity, c is the convective velocity and $u(k,t)$ is the solution expressed in the Fourier space. In LES based on solution filtering, the way to impose the filter is related to the time integration of this type of equation. In practice, the time advancement from t_n to $t_n + \Delta t$ is split into two steps, with

$$u^* = u^n + \int_{t_n}^{t_n+\Delta t} \lambda u \, dt \quad \text{(first step)} \quad , \quad u^{n+1} = T u^* \quad \text{(second step)} \tag{12}$$

with $u^n = u(k,t_n)$ and $u^{n+1} = u(k,t_n+\Delta t)$. Assuming an exact time integration for the first step, these two steps can be summarized as

$$u^{n+1} = T \exp(\lambda \Delta t) u^n \tag{13}$$

to be compared to

$$u^{n+1} = \exp(\lambda \Delta t) u^n \tag{14}$$

obtained from the exact solution of (11). The application of the filter T every time step produces a damping corresponding to an artificial dissipation as

long as $0 \leq T \leq 1$. This is precisely the desired effect in LES through the expectation that it can represent the SGS influence in the spirit of implicit LES. The damping of small scales can also be a motivation for performing DNS while controlling spurious oscillations due for instance to aliasing errors [20] or to subdomain boundaries [29].

4. Equivalence with spectral vanishing viscosity

The comparison between the time advancement (13) with its exact counterpart (14) leads to the conclusion that the deviation of T from 1 corresponds to the numerical error introduced, on purpose, by the filtering. It is easy to show that (13) also corresponds to the exact time integration of (11) with $\lambda = -ick-(\nu+\nu_s)k^2$ where ν_s can be interpreted as the SVV associated with the filtering. By the exact identification $T = \exp(-\nu_s k^2 \Delta t)$, the expression of ν_s can be obtained with

$$\nu_s(k\Delta x) = -\frac{\ln T(k\Delta x)}{k^2 \Delta t} \tag{15}$$

This very simple relation clearly shows that solution filtering can be related to an equivalent SVV, at least in a framework where time errors are neglected.

A first remark connected to this equivalence is that the value $T = 0$ is a singularity for ν_s which becomes infinite. This singularity is obtained in particular at the cutoff wavenumber k_c when $\sigma = 1$. Even if infinite values for ν_s are numerically feasible, it is difficult to relate them to any SGS contribution when interpreted in the framework of implicit LES. Another remark is related to the asymptotic behaviour of ν_s for vanishing time steps with formally

$$\lim_{\Delta t \to 0} \nu_s(k\Delta x) = \infty \quad \forall k \neq 0 \tag{16}$$

Numerically, this second singular behaviour corresponds to a loss of time consistency. It can be easily understood by remarking that a solution filtering performed in the same way every time step produces a cumulative effect that is more and more pronounced as Δt goes to zero [5].

Fortunately, both singularities can be easily avoided through a scaling of σ on the time step, enabling the application of one filtering to vanish as Δt goes to zero. For this scaling, it is convenient to introduce the numerical viscosity ν_0 which can be defined as the value of ν_s at the cutoff wavenumber with $\nu_0 = \nu_s(k_c \Delta x)$. This value can be chosen by reference to molecular

viscosity ν as explained for instance in [4] where the ratio ν_0/ν is estimated using a simplified closure of Lin's equation in the context of implicit LES. Then, σ can be adjusted on a finite value of ν_0 using expression (15) leading to

$$\sigma = 1 - \exp\left(-\nu_0 k_c^2 \Delta t\right) \tag{17}$$

This scaling of σ on Δt can restore the time consistency of the solution filtering as an alternative to the rescaling technique proposed by [5]. It also enables the control of the numerical viscosity introduced by the solution filtering for any Δt while avoiding to impose an infinite value at the cutoff wavenumber k_c. Using the Fourier number

$$F = \frac{\nu \Delta t}{\Delta x^2} \tag{18}$$

it can be convenient to make nondimensional expression (17) with

$$\sigma = 1 - \exp\left(-\pi^2 \frac{\nu_0}{\nu} F\right) \tag{19}$$

which shows that the scaled σ is only a function of ν_0/ν and F. In the same way, the nondimensional counterpart of (15) can be written as

$$\frac{\nu_s(k\Delta x)}{\nu_0} = -\frac{\ln T(k\Delta x)}{\dfrac{\nu_0}{\nu} F k^2 \Delta x^2} \tag{20}$$

To illustrate to what extent solution filtering is equivalent to SVV, the resulting $\nu_s(k\Delta x)$ are compared in figure 2-left. Here, the reference SVV corresponds to the kernel

$$\nu_s(k\Delta x) = \begin{cases} 0 & \text{if } k\Delta x < m\pi \\ \nu_0 \exp\left[-\left(\frac{\pi - k\Delta x}{m\pi - k\Delta x}\right)^2\right] & \text{if } m\pi \leq k\Delta x \leq \pi \end{cases} \tag{21}$$

with the standard value $m = 0.3$. As expected, because of its singular behaviour at the cutoff wavenumber k_c, the filter (1) based on coefficients (10) with $\sigma = 1$ is unable to mimic the standard SVV kernel. For this example, the filter is made highly selective with the value $\alpha = 0.47$ close to 0.5. Similar conclusions can be obtained from any filter based on the choice $\sigma = 1$. For instance, the optimized 6^{th}-order filter of [30], despite its good behaviour at low wavenumbers, leads to very high values of equivalent

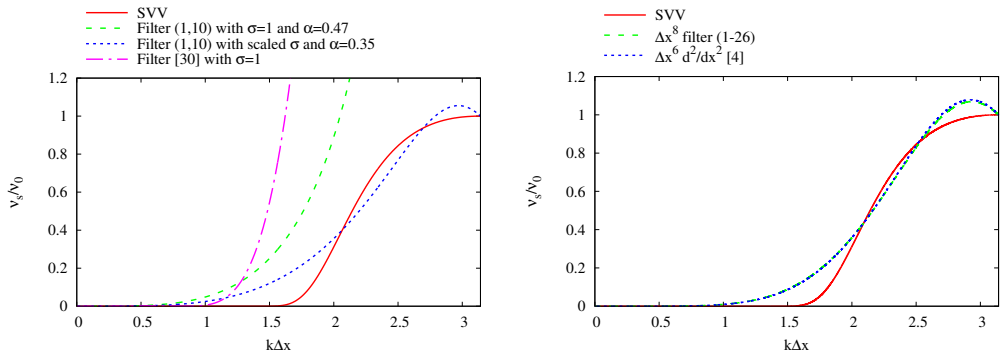

Figure 2: Left: Comparison between the reference SVV kernel and its equivalent counterparts associated to filter (1,10) with $\sigma = 1$ or with the scaling (17) and to filter [30] with $\sigma = 1$. Right: Comparison between the reference SVV kernel and its equivalent counterparts associated to filtering using (1,26) or associated to the computation of second derivative [4]. Examples at $\nu_0/\nu = 10$ and $F = 0.001$.

spectral viscosity for $k\Delta x \gtrsim 1$. This behaviour can make highly intrusive the filtering when only moderate values of the numerical viscosity are required. On the contrary, the use of the scaling (17) with $\alpha = 0.35$ leads to a kernel close to the standard SVV with a finite value at the cutoff wavenumber k_c as imposed by $\nu_0/\nu = 10$ in the example presented in figure 2-left.

So far, only 6^{th}-order filters have been considered using the set of coefficients (10). For reasons that will be explained in the following, we propose here to increase the formal order of the filter by adding the 8^{th}-order condition while using the full stencil of scheme (1). The coefficients are determined using (4-7) and to control the shape of the kernel, two extra constraints can be imposed. Here, we choose to impose the transfer function at the cutoff wavenumber k_c and at $k_m = 2k_c/3$ with $T(k_c\Delta x) = T_c$ and $T(k_m\Delta x) = T_m$. These two extra constraints can be written as

$$a_f - b_f + c_f - d_f + e_f = (1 - 2\alpha_f)T_c \tag{22}$$

$$a_f - \frac{b_f}{2} - \frac{c_f}{2} + d_f - \frac{e_f}{2} = (1 - \alpha_f)T_m \tag{23}$$

where T_c and T_m are

$$T_c = \exp\left(-\pi^2 \frac{\nu_0}{\nu} F\right) \tag{24}$$

$$T_m = \exp\left(-\frac{4\pi^2}{9} c_1 \frac{\nu_0}{\nu} F\right) \tag{25}$$

with $c_1 \approx 0.44$ as given by the SVV kernel (21) at $k = k_m$. The system of 6 equations (4–7,22,23) with the 6 unknowns $(\alpha_f, a_f, b_f, c_f, d_f, e_f)$ leads to the solution

$$\begin{aligned}
\alpha_f &= \frac{-256T_m + 81T_c + 175}{-256T_m + 162T_c + 94} \\
a_f &= \frac{T_c(35T_m + 46) - 163T_m + 82}{-128T_m + 81T_c + 47} \\
b_f &= -\frac{T_c(56T_m - 137) + 200T_m - 119}{-128T_m + 81T_c + 47} \\
c_f &= \frac{T_c(28T_m - 28) - 28T_m + 28}{-128T_m + 81T_c + 47} \\
d_f &= -\frac{T_c(8T_m - 8) - 8T_m + 8}{-128T_m + 81T_c + 47} \\
e_f &= \frac{-T_m + T_c(T_m - 1) + 1}{-128T_m + 81T_c + 47}
\end{aligned} \tag{26}$$

where T_c and T_m are given by (24,25) in which the input parameters are ν_0/ν and F.

The spectral viscosity associated to filter (1) based on the set of coefficients (26) is presented in figure 2-right. It is found to be slightly less intrusive than the 6^{th}-order filter at low wavenumbers while mimicking correctly the SVV kernel of reference. Interestingly, this spectral viscosity obtained from filtering is almost identical to the one introduced by the finite-difference scheme proposed by [4] to compute second derivatives. This remarkable similarity between filtering and second derivative opens a way for designing a filter to fully mimic a second derivative, i.e. both its numerical and molecular dissipation. This is the subject of the next section.

5. Viscous filtering

In this work, we propose a new approach where the filter is designed to provide both the molecular and artificial dissipations. Thanks to this feature, the viscous term can be removed from (11) by using $\lambda = -ick$. In this way, both the artificial and molecular dissipation have to be included in T. To enable this feature, Taylor's expansions must be performed by reference to the viscous kernel to obtain order conditions between the coefficients $(\alpha_f, a_f, b_f, c_f, d_f, e_f)$. More precisely, the purpose is to approach the exact

amplification factor associated with the purely diffusive case,

$$T_{\text{ref}} = \exp(-\nu k^2 \Delta t) = \exp\left[-F(k\Delta x)^2\right] \tag{27}$$

with a given order of accuracy. Taylor's expansions of (27), of the numerator and denominator of (2) lead respectively to

$$\exp\left[-F(k\Delta x)^2\right] = 1 - F(k\Delta x)^2 + \frac{F^2(k\Delta x)^4}{2!} - \frac{F^3(k\Delta x)^6}{3!} + O(k\Delta x)^8, \tag{28}$$

$$1 + 2\alpha_f \cos(k\Delta x) = 1 + 2\alpha_f \left[1 - \frac{(k\Delta x)^2}{2!} + \frac{(k\Delta x)^4}{4!} - \frac{(k\Delta x)^6}{6!}\right] + O(k\Delta x)^8 \tag{29}$$

and

$$\begin{aligned}
a_f &+ b_f \cos(k\Delta x) + c_f \cos(2k\Delta x) + d_f \cos(3k\Delta x) + e_f \cos(4k\Delta x) = \\
a_f &+ b_f \left[1 - \frac{(k\Delta x)^2}{2!} + \frac{(k\Delta x)^4}{4!} - \frac{(k\Delta x)^6}{6!}\right] \\
&+ c_f \left[1 - \frac{2^2(k\Delta x)^2}{2!} + \frac{2^4(k\Delta x)^4}{4!} - \frac{2^6(k\Delta x)^6}{6!}\right] \\
&+ d_f \left[1 - \frac{3^2(k\Delta x)^2}{2!} + \frac{3^4(k\Delta x)^4}{4!} - \frac{3^6(k\Delta x)^6}{6!}\right] \\
&+ e_f \left[1 - \frac{4^2(k\Delta x)^2}{2!} + \frac{4^4(k\Delta x)^4}{4!} - \frac{4^6(k\Delta x)^6}{6!}\right] + O(k\Delta x)^8
\end{aligned} \tag{30}$$

Then, by identification order by order of (2) with (27), the following set of conditions is obtained with

$$\begin{aligned}
1 + 2\alpha_f &= a_f + b_f + c_f + d_f + e_f && (\Delta x^2) \\
2F(1 + 2\alpha_f) + 2\alpha_f &= b_f + 4c_f + 9d_f + 16e_f && (\Delta x^4) \\
12F^2(1 + 2\alpha_f) + 24F\alpha_f + 2\alpha_f &= b_f + 16c_f + 81d_f + 256e_f && (\Delta x^6) \\
120F^3(1 + 2\alpha_f) + 360F^2\alpha_f + 60F\alpha_f + 2\alpha_f &= b_f + 64c_f + 729d_f + 4096e_f && (\Delta x^8)
\end{aligned} \tag{31}$$

Naturally, for the inviscid case given by $F = 0$ (i.e. $T_{ref} = 1$), conditions (4-7) are recovered. For the more general viscous case ($F \neq 0$), as in the previous section, we have 6 coefficients $(\alpha_f, a_f, b_f, c_f, d_f, e_f)$ subjected to the 4 conditions (31).

A first option is to remove 2 coefficients, with $d_f = e_f = 0$ in order to make more compact the resulting scheme. Contrary to a standard filter based on conditions (4-7), the present new type of filter, which can be designated as a *viscous filter*, is self-sufficient without requiring any extra condition to avoid the singular solution $a_f = 1$, $\alpha_f = b_f = c_f = 0$. The solving of the corresponding system (31) leads to the set of coefficients

$$\begin{aligned}
\alpha_f &= -\frac{30F^2 - 15F + 2}{60F^2 + 60F - 11} \\
a_f &= \frac{180F^3 - 240F^2 + 171F - 22}{120F^2 + 120F - 22} \\
b_f &= -\frac{120F^3 - 120F^2 - 6F + 4}{60F^2 + 60F - 11} \\
c_f &= \frac{60F^3 - 3F}{120F^2 + 120F - 22}, \quad d_f = 0, \quad e_f = 0
\end{aligned} \tag{32}$$

The associated modified square wavenumber k'' given by

$$k''\Delta x^2 = -\frac{\ln T}{F} \tag{33}$$

is compared in figure 3-left to the exact differentiation $k'' = k^2$ and to the modified square wavenumber of the very popular 6^{th}-order scheme of [28] for the computation of the second derivative. The almost perfect collapse between viscous filtering and second derivative suggest that these two finite-difference techniques can produce very similar results to represent physical diffusion. The former can be seen as the counterpart of the latter while including the time integration. This point will be discussed more in the next section and also in Appendix A.

The comparison presented in figure 3-left is based on a low value of the Fourier number $F = 0.001$. Lower values of F would produce virtually identical k''. The use of higher values has to be discussed more carefully. First, it can be noticed that all the coefficients (32) become singular for the positive root of their denominator given by $F = \dfrac{\sqrt{390} - 15}{30} \approx 0.158$. In practice, in the neighbourhood of this singularity, the transfer function $T(k\Delta x)$ becomes erratic with strong deviations from its exact reference $\exp(-\nu k^2 \Delta t)$ and sudden changes of sign (with vertical asymptotes) at particular wavenumbers k. In this range of F, this filtering technique becomes inoperable. In a more

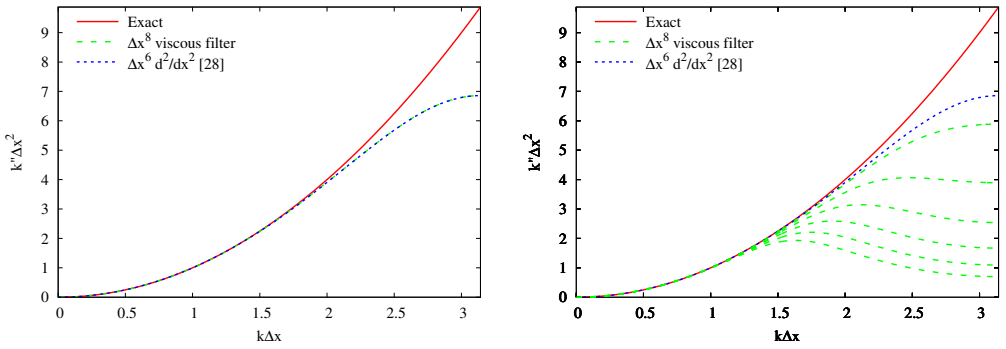

Figure 3: Comparison between the exact wavenumber and its modified counterparts associated to viscous filtering or to the computation of second derivative. Left: $F = 0.001$ (green-dashed curve). Right: F from 0.5 to 1 by step of 0.1 (from top to bottom green-dashed curves).

general way, because $T(k\Delta x)$ corresponds to the amplification factor in the context of von Neumann stability analysis, the present scheme is numerically stable if $|T(k)| \leq 1$. To exhibit its numerical stability, the isocontour $T = 1^+$ in the plane $(k\Delta x, F)$ is presented in figure 4. A very thin unstable zone can be identified near the singularity $F \approx 0.158$ suggesting to avoid the range $0.14 < F < 0.17$. For higher values of F, another unstable zone can be noticed, starting from $F > 1.35$ at $k = k_c$.

Even if the present scheme is numerically stable at $F \approx 1$, it is worth to address its accuracy. For that purpose, a map of the error parameter $k''_{\text{err}} = \dfrac{k'' - k^2}{k_c^2}$ in the plane $(k\Delta x, F)$ is presented in figure 5. Paradoxically, the unstable/inaccurate zone (plotted in red) near $F \approx 0.158$ is surrounded by regions where the accuracy is slightly improved by reference to the error at low F. Outside the unstable/inaccurate range $F \in]0.14, 0.17[$, low values $F \leq 0.14$ provide similar accuracy. On the contrary, high values $F \geq 0.14$ deteriorate the accuracy as F is increased, with a strong under-estimation of k'' at high wavenumber $k\Delta x \in [\pi/2, \pi]$. This behaviour is also illustrated in figure 3-right in the range $0.5 \leq F \leq 1$. Based on these observations, it is suggested that the useful ranges of Fourier number to ensure both stability and accuracy are $F \leq 0.14$ and $0.17 \leq F \leq 0.5$.

To avoid the singular behaviour of the scheme because of the root of its coefficient denominator, it can be decided to make it explicit ($\alpha_f = 0$) while

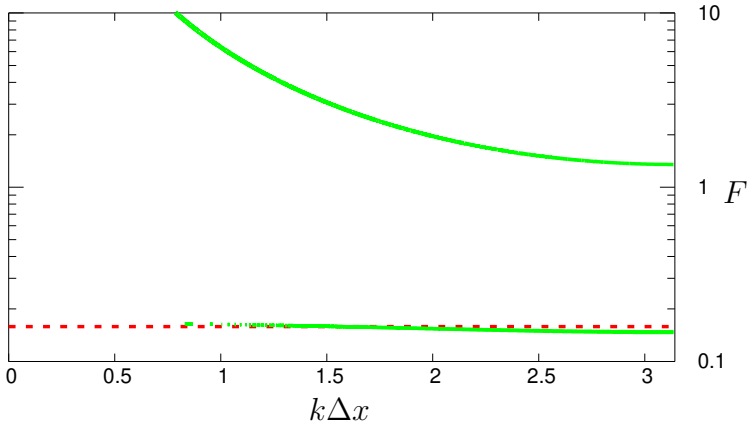

Figure 4: Isocontour $T = 1^+$ in the plane $(k\Delta x, F)$. The red dashed line indicates the singular value $F \approx 0.158$.

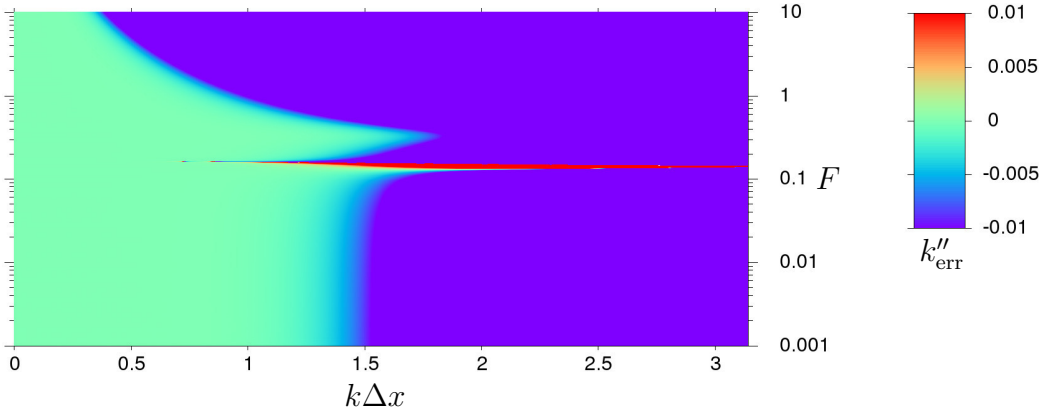

Figure 5: Map of the error parameter $k''_{\text{err}} = \dfrac{k'' - k^2}{k_c^2}$ in the plane $(k\Delta x, F)$. Saturated colormap for $|k''_{\text{err}}| > 1\%$.

extending its stencil ($d_f \neq 0$) in order to preserve the 8^{th}-order accuracy. With these new constraints, solving system (31) leads to

$$\begin{aligned} a_f &= -\frac{60F^3 - 84F^2 + 49F - 18}{18} \\ b_f &= \frac{10F^3 - 13F^2 + 6F}{2} \\ c_f &= -\frac{20F^3 - 20F^2 + 3F}{10} \\ d_f &= \frac{30F^3 - 15F^2 + 2F}{90}, \quad \alpha_f = 0, \quad e_f = 0 \end{aligned} \tag{34}$$

A second alternative is to keep its implicit feature ($\alpha_f \neq 0$) while using the stencil extension ($d_f \neq 0$) to ensure an extra constraint designed to impose the transfer function at k_c as in (22). In that case, to take into account both the molecular and numerical viscosities, T_c is given by

$$T_c = \exp\left[-\pi^2 \left(\frac{\nu_0}{\nu} + 1\right) F\right] \tag{35}$$

instead of (24) which was designed to only mimic the numerical dissipation. These extra constraint combined with system (31) leads to the solution

$$\begin{aligned} \alpha_f &= -\frac{45T_c + 480F^3 - 600F^2 + 272F - 45}{-90T_c + 960F^3 + 240F^2 - 416F + 90} \\ a_f &= \frac{F^3(600T_c - 720) + F(145T_c - 561) - 90T_c + F^2(1158 - 390T_c) + 240F^4 + 90}{-90T_c + 960F^3 + 240F^2 - 416F + 90} \\ b_f &= -\frac{F^3(1800T_c - 240) + F(135T_c + 953) + 180T_c + F^2(-990T_c - 1362) + 240F^4 - 180}{-180T_c + 1920F^3 + 480F^2 - 832F + 180} \\ c_f &= -\frac{F^2(90T_c + 438) + F(81T_c - 81) + F^3(-360T_c - 720) + 240F^4}{-90T_c + 960F^3 + 240F^2 - 416F + 90} \\ d_f &= \frac{F(7T_c - 7) + F^2(78 - 30T_c) + F^3(-120T_c - 240) + 240F^4}{-180T_c + 1920F^3 + 480F^2 - 832F + 180}, \quad e_f = 0 \end{aligned} \tag{36}$$

Both sets of coefficients (34) and (36) avoid any erratic behaviour around a singular value of F. The stability condition is more favourable for the scheme (1,36) than for the scheme (1,34) with $F < 4.12$ for the former and $F < 0.84$ for the latter. More importantly, at 10% of the maximum stable Fourier number, the scheme (1,36) is significantly more accurate than the scheme (1,34) as illustrated in figure 6-left.

Following the method presented in the previous section to control the shape of the SVV kernel introduced by the filtering, the last option presented

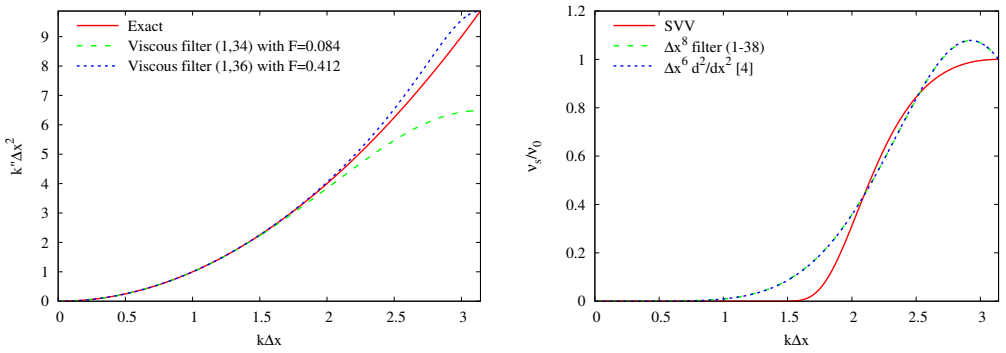

Figure 6: Left: Comparison between schemes (1,34) and (1,36) at 10% of the maximum stable Fourier number F ($\nu_0/\nu = 0$). Right: Comparison between the reference SVV kernel and its equivalent counterparts associated to filtering using (1,38) or to the computation of second derivative [4] ($\nu_0/\nu = 10$ and $F = 0.001$).

here is to use the full stencil ($d_f \neq 0$ and $e_f \neq 0$) of scheme (1) while imposing the transfer function at k_c and k_m through the two constraints (22,23) where T_c is given by (35) and T_m by

$$T_m = \exp\left[-\frac{4\pi^2}{9}\left(c_1\frac{\nu_0}{\nu}+1\right)F\right] \tag{37}$$

Then, solving system (31,22,23) provides the set of coefficients

$$
\begin{aligned}
\alpha_f &= -\frac{1280T_m - 405T_c + 1440F^3 - 3240F^2 + 2736F - 875}{-1280T_m + 810T_c + 2880F^3 - 2160F^2 - 288F + 470} \\
a_f &= \frac{\left(\begin{array}{l} F(3520T_m + 855T_c - 4951) + F^3(3200T_m + 1800T_c - 1520) + \\ T_c(700T_m + 920) - 3260T_m + F^2(-4640T_m - 2430T_c + 5038) + 240F^4 + 1640 \end{array}\right)}{-2560T_m + 1620T_c + 5760F^3 - 4320F^2 - 576F + 940} \\
b_f &= \frac{\left(\begin{array}{l} F^2(2560T_m + 6210T_c + 6478) + F(256T_m - 4329T_c - 6871) - 4000T_m + \\ T_c(2740 - 1120T_m) + F^3(-2560T_m - 3960T_c - 1520) + 240F^4 + 2380 \end{array}\right)}{-2560T_m + 1620T_c + 5760F^3 - 4320F^2 - 576F + 940} \\
c_f &= -\frac{\left(\begin{array}{l} F(1792T_m - 2115T_c + 323) + F^3(1280T_m - 1800T_c - 1040) + 280T_m + \\ T_c(280 - 280T_m) + F^2(-2240T_m + 2970T_c + 598) + 240F^4 - 280 \end{array}\right)}{-1280T_m + 810T_c + 2880F^3 - 2160F^2 - 288F + 470} \\
d_f &= -\frac{\left(\begin{array}{l} F^2(2560T_m - 2430T_c + 2158) + F(256T_m + 855T_c - 1111) + \\ T_c(160T_m - 160) - 160T_m + F^3(-2560T_m + 1800T_c - 1520) + 240F^4 + 160 \end{array}\right)}{-2560T_m + 1620T_c + 5760F^3 - 4320F^2 - 576F + 940} \\
e_f &= \frac{\left(\begin{array}{l} F^2(160T_m - 270T_c + 478) + F(64T_m + 99T_c - 163) + \\ T_c(20T_m - 20) - 20T_m + F^3(-640T_m + 360T_c - 560) + 240F^4 + 20 \end{array}\right)}{-2560T_m + 1620T_c + 5760F^3 - 4320F^2 - 576F + 940}
\end{aligned}
\tag{38}
$$

The corresponding SVV can be expressed using this time the exact identification $T = \exp[-(\nu + \nu_s)k^2\Delta t]$ in order to incorporate both the molecular and artificial dissipations while solving (11) with $\lambda = -ick$. Then, the counterpart of (15) becomes

$$
\nu + \nu_s(k\Delta x) = -\frac{\ln T(k\Delta x)}{k^2\Delta t} \tag{39}
$$

or equivalently in nondimensional form

$$
\frac{\nu_s(k\Delta x)}{\nu_0} = -\frac{\ln T(k\Delta x)}{\frac{\nu_0}{\nu} F k^2 \Delta x^2} - \frac{\nu}{\nu_0} \tag{40}
$$

As in the previous section, when compared with the approach of [4] based on the explicit computation of the viscous term while boosting it artificially at small scales, the present viscous filtering method can lead to virtually identical spectral viscosity as shown in figure 6-right. Both approaches can behave like SVV with an equivalent flexibility through the choice of the input parameters ν_0/ν and c_1 to shape the associated kernel. In terms of stability,

the extra constraint at k_m introduces an unstable range $0.023 < F < 0.64$. For higher values of F, numerical stability is ensured as long as $F < 7.94$ but with a strong loss of accuracy (not shown for conciseness). Even if the stability condition $F < 0.023$ is more restrictive than for schemes (34) and (36), it is not at all penalizing in many DNS/LES applications where the typical values of Fourier numbers are clearly smaller.

By comparison to conventional filtering, the present viscous filtering technique enables the bypass of the viscous term and then the saving of computational time. But in terms of computational efficiency, the main advantage of viscous filtering lies in its robustness for large values of the Fourier number F. This fundamental point is discussed in the following section through an analysis of the formal accuracy and numerical stability of this new approach.

6. Accuracy analysis

To validate the present viscous filtering procedure while exhibiting its main accuracy features, the standard convection/diffusion equation

$$\frac{\partial u}{\partial t} + c\frac{\partial u}{\partial x} = \nu\frac{\partial^2 u}{\partial x^2} \tag{41}$$

is solved where $u(x,t)$ is the solution expressed in the physical space. With the initial condition

$$u(x,0) = \exp\left[-\left(\frac{x - L_x/2}{\sigma_x}\right)^2\right] \tag{42}$$

this equation has an exact solution with

$$u(x,t) = \sqrt{\frac{\sigma_x^2}{\sigma_x^2 + 4\nu t}}\exp\left[-\frac{(x - ct - L_x/2)^2}{\sigma_x^2 + 4\nu t}\right] \tag{43}$$

where L_x is the computational domain considered. The problem is solved using periodicity in x while considering a narrow Gaussian with $\sigma_x = L_x/40$ to make negligible the role of the boundary condition for the deviation from the exact solution (43) subjected to same periodicity. Using the nondimensionalisation $L_x = 1$ and $c = 1$, the viscosity considered is $\nu = 1/1000$ and the equation is solved up to $t = 1$.

In this section, we want to address the general features of the viscous filtering by comparison to the conventional approach where the viscosity effects are described through the computation of the right hand side of equation (41) using a finite-difference scheme for the computation of the second derivative. For this classical way to take viscous effects into account, we will refer to explicit diffusion. As generic viscous filter operator, only the scheme given by the set of coefficients (36) is considered for conciseness. In the same way, as generic second derivative scheme, only the 6^{th}-order scheme reported in [23] is used for comparisons. These two schemes are expected to behave very closely as it was observed in the previous section and as it will be checked practically in this section. To reduce the spatial differentiation errors, both schemes are scaled to provide a very small amount of numerical dissipation using $\nu_0/\nu = 0$. This choice to consider only these two schemes is for conciseness reasons. Fundamentally, all the comparisons discussed in what follows can be transposed for other numerical parameters (accuracy order, stencil, imposition of T_c and T_m, etc.) provided that the viscous filter is compared to its counterpart for the computation of the second derivative.

6.1. Spatial accuracy

First, the spatial accuracy is addressed by using a very small time step Δt making negligible the error due to the time integration. For the conventional approach, the advancement is entirely based on a 3^{rd}-order Adams-Bashforth (AB3) scheme. For the technique based on viscous filtering, the AB3 scheme is only used for the convective term while representing the diffusion by the application of the viscous filter operator on the computed solution every time step as explained in section 3. In both cases, the spatial differentiation of the convective term is performed using the same 6^{th}-order compact finite-difference scheme (see [28, 31] for information on this standard centred scheme for the computation of first derivative).

The spatial convergence obtained in each case is shown in figure 7 by considering both the convective/diffusive ($c = 1$) and purely diffusive ($c = 0$) situations. Three spatial resolutions have been considered with $\Delta x = L_x/n_x$ where n_x is the number of mesh nodes with $n_x = 256, 512, 1024$. The remarkable matching of the L_2-norm at any spatial resolution clearly confirms that the present viscous filtering technique can mimic almost perfectly an explicit diffusion. A 6^{th}-order accuracy is well recovered. This accuracy order of the viscous filter (1,36) is expected in view of the almost perfect

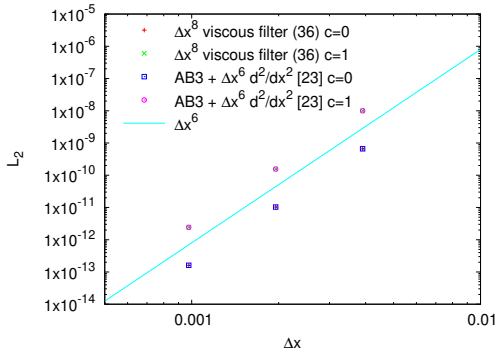

Figure 7: Spatial convergence for diffusion ($c = 0$) and convection/diffusion ($c = 1$) equations. Comparison between the present viscous filtering technique and the conventional explicit computation of the diffusion term. Three spatial resolutions are considered with $\Delta x = L_x/n_x$ and $n_x = 256, 512, 1024$.

collapse between modified wavenumbers as illustrated in figure 3[1]. However, the 6^{th}-order accuracy may seem like a contradiction in view of the order conditions checked up the 8^{th} order as expressed in (31). In practice, it is worth noting that the 8^{th}-order accuracy is ensured only if F is kept constant with the same number of time steps. For the present investigation of spatial convergence based on a constant time step Δt while computing the L_2-norm at the same time $t = 1$, the variation of F, as Δx is reduced, introduces a division by Δx^2 of the numerical error, explaining the 6^{th}-order accuracy observed in the present tests of spatial convergence. This is the reason why a Δx^8 formulation corresponds in practice to a 6^{th}-order accuracy in terms of spatial convergence. Note that it can be checked that the computation of the L_2-norm based on a spatial convergence at $F = \text{cst}$ with the same number of time steps leads to L_2-norm $\propto \Delta x^8$ as expected (not shown for conciseness). In Appendix A, the reason of this reduction by Δx^2 of the formal order is exhibited analytically.

[1]Figure 3 actually compares the modified wavenumber of the viscous filter (32) with its second derivative counterpart, but the same agreement (not shown for conciseness) can be obtained for the viscous filter (36) used in the present validation.

6.2. Temporal accuracy

The accuracy in time of the two strategies, namely the viscous filtering and the explicit diffusion, is more difficult to assess. This difficulty is related to the impossibility to make negligible the contribution of the spatial error. For the conventional method based on the explicit computation of the diffusion term, in the framework of von Neumann analysis, it is well known that numerical stability is ensured only if

$$F < \frac{\sigma_r}{k''_{\max}\Delta x^2} \tag{44}$$

where $k''_{\max}\Delta x^2$ is the maximum of the modified square wavenumber while σ_r is a feature of the time advancement scheme with $\sigma_r = 6/11$ for the AB3 scheme used in this study [32]. In the present formalism, $k''_{\max}\Delta x^2 = (1+\nu_0/\nu)\pi^2$ leads to the Fourier stability condition

$$F < \frac{6}{11(1+\nu_0/\nu)\pi^2}. \tag{45}$$

which reads $F \lesssim 0.055$ for $\nu_0/\nu = 0$. Close to this critical value, thanks to the accuracy of the AB3 scheme, the main contribution to the numerical error comes from the spatial discretisation. A mesh refinement while keeping constant Δt is a way to remove progressively the spatial differentiation error by comparison to the temporal error, but the resulting higher value of F leads to numerical instability, making impossible the evaluation of the time accuracy. To ensure numerical stability, a mesh refinement by a factor 2 requires a reduction of the time step by a factor 4 because of the scaling of F on $1/\Delta x^2$. Then, for the present combination $(\Delta x^6, \Delta t^3)$, the balance between time and spatial errors is kept constant, making impossible a time convergence analysis based on a negligible contribution of the spatial differentiation error.

To overcome this difficulty, the present assessment is based on local accuracy. The principle of local accuracy analysis is to estimate the numerical error introduced only by one time step ($n_t = 1$), in contrast to global accuracy for which the numerical convergence is examined by considering the solution at a given time t while decreasing the time step Δt (i.e. by increasing the number of time steps n_t with $t = n_t\Delta t$). The advantage of local accuracy analysis is that it is not restricted to the stability zone of the scheme, enabling the investigation of high values of F. In present analysis,

this convenient property can be used to make negligible the contribution of spatial errors. Local accuracy is connected to global accuracy such that a Δt^n-accurate time scheme exhibits a local convergence proportional to Δt^{n+1}. As a consequence, for the present AB3 scheme, a Δt^4 local convergence is expected. To check this scaling, equation (41) has been advanced in time for one time step Δt using a spatial resolution with $n_x = 512$. To relate more easily the range of considered Δt with the AB3 stability condition $F \lesssim 0.055$, the convergence is exhibited as a scaling in F, a global 3^{rd}-order accuracy corresponding to a F^4 scaling.

Figure 8 compares the local time convergence of the present viscous filtering technique with the conventional approach where the viscous term is computed explicitly by spatial differentiation (second derivative). To start this analysis, the simpler case of the pure diffusion ($c = 0$) is first addressed. For the explicit diffusion, two zones can be distinguished in figure 8-left. From very small F to $F \approx 0.05$, a scaling in F can be clearly noticed. It corresponds to a lack of numerical convergence in terms of global accuracy. This behaviour corresponds to the situation already discussed for which the spatial errors completely dominate the time errors, preventing any convergence in time. At higher F, a scaling in F^4 is established, confirming the 3^{rd}-order accuracy of the AB3 scheme. In this second zone, beyond the stability region, it can be considered that the contribution of spatial error is negligible.

The behaviour of the time error for the viscous filtering also exhibits the non-convergence zone at small F but reveals a more complex behaviour for $F \gtrsim 0.05$. Fortunately, the more or less erratic behaviour of the time error with F in the range $0.1 \lesssim F \lesssim 1$ corresponds to an increase of the accuracy. A more regular dependency on F is recovered for $F \gtrsim 1$ with a scaling close to F^4 corresponding to a global 3^{rd}-order accuracy. The lack of a clear scaling in F is an expected result because of the entanglement between time and spatial errors which is an essential feature of the present viscous filter scheme. The present analysis shows that this feature is not a drawback thanks to the resulting time accuracy which is clearly improved by comparison to the AB3 scheme. In the zone where time error dominates, namely for $F \gtrsim 0.05$, the improvement corresponds to a reduction of about one order of magnitude in the error. At lower F, this reduction is gradually removed, as the contribution of the time error by comparison to the spatial error, but the viscous filtering remains the most accurate approach. As a first conclusion, for the purely diffusive case, it can be stated that the

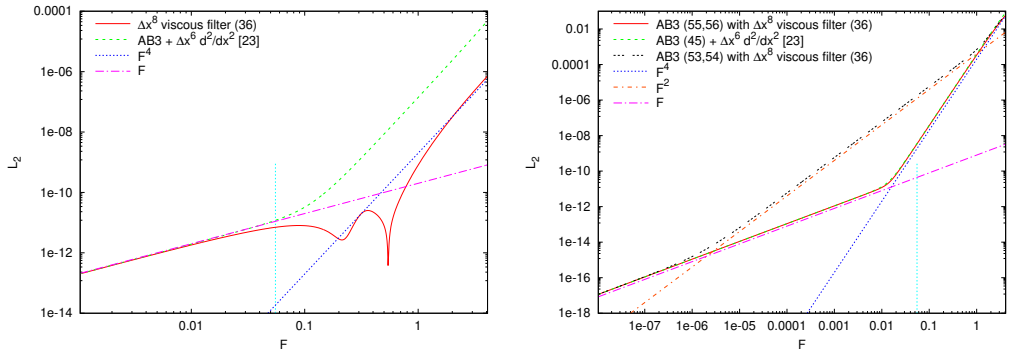

Figure 8: Local time convergence exhibited as a scaling in F. Left: diffusion ($c = 0$) equation. Right: convection/diffusion ($c = 1$) equation. Comparison between the present viscous filtering technique and the conventional explicit computation of the diffusion term. The blue dashed line indicates the stability limit of the AB3 scheme $F \lesssim 0.055$.

viscous filtering technique is more accurate in time than the AB3 scheme. This feature is of secondary importance at low F for which spatial error dominates. At higher F, the accuracy improvement is a favourable property that supplements the numerical stability which is already a major advantage.

The convective/diffusive case ($c = 1$) must be considered more carefully. In this situation, both approaches (viscous filtering and explicit diffusion) require the time integration of the convective term. For the present technique based on viscous filtering, the way to accurately combine the time integration of the convective term and the application of the filter (in which the time integration is embedded) needs to be clarified. In the general case, the convective term may be non-linear requiring an approximation for the time advancement. The corresponding generic equation, written in the Fourier space, reads as

$$\frac{du}{dt} = F(u) - \nu k^2 u \tag{46}$$

To integrate this equation in time, a simple option is to treat the two terms on the right hand side using the same scheme, with, in the case of an explicit multi-step scheme

$$u^{n+1} = u^n + \Delta t \sum_{i=0}^{p} a_i \left[F(u^{n-i}) - \nu k^2 u^{n-i} \right] \tag{47}$$

for which the AB3 scheme coefficients are given by $p = 2$, $a_0 = 23/12$, $a_1 = -16/12$ and $a_2 = 5/12$. This technique, referred here as the conventional strategy, does not require any filtering given the explicit computation of the diffusion term.

If one desires to integrate exactly the viscous term while approximating the non-linear term with a multi-step scheme, it may be tempting to split the time advancement into two steps with

$$u^* = u^n + \Delta t \sum_{i=0}^{p} a_i F(u^{n-i}) \tag{48}$$

$$u^{n+1} = \exp(-\nu k^2 \Delta t) u^* \tag{49}$$

The drawback of this approach is that a time splitting error is introduced preventing from considering as exact the time advancement of the viscous term in the second step (49). To integrate exactly the viscous term, equation (46) can be multiplied by the so-called integrating factor [33, 34] $\exp(\nu k^2 t)$ leading to

$$\frac{d[u \exp(\nu k^2 t)]}{dt} = F(u) \exp(\nu k^2 t) \tag{50}$$

Then, the time advancement scheme no longer requires a splitting with

$$u^{n+1} \exp(\nu k^2 t_{n+1}) = u^n \exp(\nu k^2 t_n) + \Delta t \sum_{i=0}^{p} a_i \exp(\nu k^2 t_{n-i}) F(u^{n-i}) \tag{51}$$

or, after division by $\exp(\nu k^2 t_{n+1})$,

$$u^{n+1} = \exp(-\nu k^2 \Delta t) \left[u^n + \Delta t \sum_{i=0}^{p} a_i \exp(-i\nu k^2 \Delta t) F(u^{n-i}) \right] \tag{52}$$

Expressed into two steps, as a more convenient way to implement it, this time advancement can be written as

$$u^* = u^n + \Delta t \sum_{i=0}^{p} a_i \exp(-i\nu k^2 \Delta t) F(u^{n-i}) \tag{53}$$

$$u^{n+1} = \exp(-\nu k^2 \Delta t) u^* \tag{54}$$

without introducing any time splitting error.

The exact amplification factor (27) is recovered in these two steps. Because the present approach consists in the approximation of this amplification factor by a discrete filtering operator of transfer function T, the analogous of the two-step time advancements (48,49) and (53,54) are respectively

$$u^* = u^n + \Delta t \sum_{i=0}^{p} a_i F(u^{n-i}) \tag{55}$$

$$u^{n+1} = Tu^* \tag{56}$$

and

$$u^* = u^n + \Delta t \sum_{i=0}^{p} a_i T^i F(u^{n-i}) \tag{57}$$

$$u^{n+1} = Tu^* \tag{58}$$

The advantage of (55,56) is that it only requires one filtering per time step. In the present framework of finite-difference schemes, the computational cost of this type of filter is equivalent to that of a second derivative, avoiding any extra-cost due to the viscous filtering strategy. The drawback is the time splitting error resulting in a loss of time accuracy. The time advancement (57,58), free from any time splitting error, is more accurate but also more expensive through the need to filter three times per time step for an AB3 scheme: twice in (57) and once in (58). By comparison to the computation of one second derivative, the extra-cost is 200%. This may be seen as very penalizing, but as it will be discussed in the next session, when implemented in a full Navier-Stokes solver, the relative extra-cost brought about by the viscous filtering is much lower while offering very advantageous features in terms of numerical stability.

Figure 8-right presents the local convergence obtained for the convection/diffusion equation. For the present balance between convection and diffusion given by $c = 1$ and $\nu = 1/1000$, the time accuracy is mainly driven by the time integration of the convective term. As a consequence, schemes (47) and (57,58) are close to each other with a global 3^{rd}-order accuracy (i.e. a scaling of the local error in F^4) provided by the AB3 scheme for $F \gtrsim 0.01$. For lower values of F, the time convergence saturates because of the spatial errors as indicated by the scaling in F. The loss of accuracy using the scheme (55,56) is clearly exhibited in figure 8-right with a scaling in F^2 (i.e. global 1^{st}-order accuracy) in the extended range $10^{-5} \lesssim F \lesssim 1$. For the present

accuracy analysis performed with very low spatial errors, the superiority of scheme (57,58) by comparison to scheme (55,56) is clearly shown. However, the time splitting error of scheme (55,56) can become insignificant in the context of multidimensional non-linear governing equations. The generalisation of present viscous filtering in this more demanding context is the main subject of the next section.

7. DNS/LES results

In this section, the present viscous filtering technique is used to perform DNS/LES of two academic turbulent flows. The corresponding scheme has been implemented in the finite-difference code Incompact3d that numerically solves the incompressible Navier-Stokes equations. This code is massively parallel and 6^{th}-order accurate in space when free-slip or periodic boundary conditions are used, as in the present study. The computational mesh is Cartesian with $n_x \times n_y \times n_z$ nodes regularly distributed in the domain $L_x \times L_y \times L_z$[2]. For more information about this code, the reader is referred to [31, 35, 36] and also to [37] for an extension of its capabilities in the new framework called Xcompact3D.

The implementation of the viscous filter in Incompact3d was straightforward thanks to the generic form of the finite-difference scheme (1). The only sensitive point is to carefully code the sets of coefficients, e.g. (36) or (38), as functions of F and ν_0/ν given the dependency of T_c and T_m on these two parameters. Note that these two sets of coefficients preserve the 6^{th}-order accuracy of Incompact3d.

When the Navier-Stokes equations are solved in the conventional way through the explicit computation of the second derivatives in the viscous term while integrating in time the governing equations as in (47), we will refer to "Navier-Stokes" results. When the viscous filtering is used, because the viscous term is removed from the governing equations, the corresponding results will be designated by the term "Euler+VF" with VF designating Viscous Filtering. More precisely, we will make the distinction between "Euler+VF^1" and "Euler+VF^3" to refer to a time advancement based respectively on one VF (55,56) or three VF (57,58) operations per time step.

In what follows, the goal is to assess the concept of viscous filtering in the general framework of high-fidelity simulation of turbulent flows. Subsec-

[2]The mesh refinement in one direction, enabled by Incompact3d, is not used here.

tion 7.1 is mainly a validation based on a widely documented fundamental flow in order to show the remarkable equivalence between a computation based on "Navier-Stokes" or "Euler+VF" formulations. Then, a problem with wall turbulence and heat transfer is addressed in subsection 7.2. The equivalence between "Navier-Stokes" and "Euler+VF" formulations is also well recovered, but more importantly, the interest of "Euler+VF" approach is evidenced through its high computational efficiency for numerical stability reasons.

7.1. Taylor-Green Vortex problem

In this subsection, the Taylor-Green Vortex (TGV) problem is used as a benchmark to assess the present viscous filtering technique. The corresponding solution is triperiodic in a cubic domain $(2\pi)^3$. Two Reynolds numbers $Re = 1/\nu$ are addressed from $t = 0$ to $t = 20$. In this time interval, the flow is subjected to a strong turbulent breakdown up to a fully developed state of turbulence. Formally, the low Reynolds number case $Re = 1250$ may not be seen as turbulent because of the deterministic nature of the flow evolution. However, a multiscale state is well established at $t = 20$, as an important feature in common with turbulence. The advantage of the deterministic dynamics is that it enables an easy assessment of the numerical accuracy based on instantaneous states obtained by DNS. For the higher Reynolds number $Re = 10000$ considered, this attractive feature is lost because of non-deterministic evolution of the flow after the turbulent breakdown. In this second framework, the LES capabilities of the present viscous filter will be examined more qualitatively.

At $Re = 1250$, using a spatial resolution of 480^3 nodes[3], the DNS accuracy is fully reached. Figure 9-left compares the time evolution of the kinetic energy E_k for the conventional "Navier-Stokes" strategy and for the present "Euler+VF^1" and "Euler+VF^3" alternatives. The former is based on the second derivative scheme documented in [23] whereas in the two latter cases, the viscous filter is given by (1,36). As already mentioned and checked in section 6, these two finite-difference schemes are expected to behave almost identically for the discrete representation of viscous effects as well as the slight artificial dissipation using $\nu_0/\nu = 3$ to control aliasing errors. The

[3]The symmetries of the problem has been used to reduce by a factor 8 the number of degrees of freedom actually computed in the impermeable sub-box π^3.

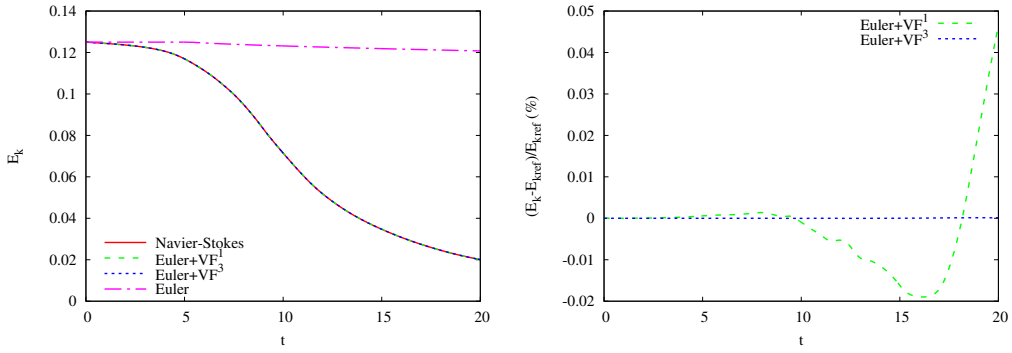

Figure 9: Time evolution of the kinetic energy E_k (left) and its relative error $\frac{E_k - E_{k\,\mathrm{ref}}}{E_{k\,\mathrm{ref}}}$ in % (right).

collapse between the three curves in figure 9-left confirms this point. The viscous dissipation, that drives the free decay of this turbulence problem, is found to be numerically equivalent for the three approaches. Thanks to the deterministic nature of the flow, defining the reference solution as the one obtained from the "Navier-Stokes" formulation, the relative deviation $\frac{E_k - E_{k\,\mathrm{ref}}}{E_{k\,\mathrm{ref}}}$ can be monitored throughout the simulation. Figure 9-right compares the time evolution of this deviation. For the "Euler+VF^1" case, the maximum deviation of about 0.045% remains acceptable without compromising the DNS accuracy. However, it can be observed that the "Euler+VF^3" strategy enables a drastic improvement of the agreement with the reference solution through a reduction of the maximum deviation by more than 300. This behaviour is consistent with the results reported in subsection 6.2 where the clear improvement of accuracy was observed using the time advancement scheme (57,58) by comparison to (55,56).

The "Euler" case is also presented in figure 9 to exhibit the behaviour of the code Incompact3d when computing a discrete solution free from any viscous effect. Thanks to the use of the skew-symmetric form for the convective terms, this code can ensure the kinetic energy conservation up to the time integration error. Using the same time step as for the three other cases, a slight decrease of E_k can be observed beyond the start of the turbulent breakdown due to the time error associated to the AB3 scheme. The use of a smaller time step can easily make insignificant this deviation from a pure kinetic energy conservation (not shown).

The multiscale dynamics produced at $t = 14$, after the turbulence break-

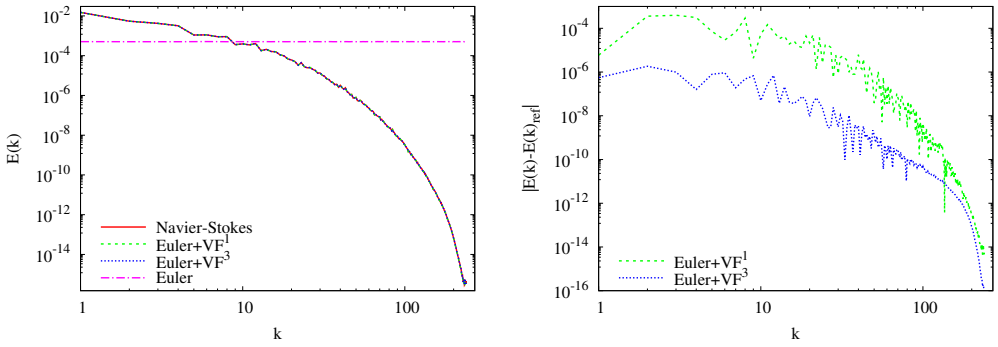

Figure 10: Kinetic energy spectra $E(k)$ (left) and its absolute error $|E(k)-E(k)_{\text{ref}}|$ (right) at $t = 14$.

down, is illustrated in figure 10-left where the kinetic energy spectra $E(k)$ are presented. For the "Euler" case, a flat spectrum corresponding to a white noise can be clearly observed, as expected. The excellent agreement between the three other strategies is well recovered on the whole range of wavenumbers k, confirming practically the equivalence between the present viscous filtering and the conventional technique where the viscous term is computed explicitly. The quality of this agreement is particularly remarkable at the smallest scales captured by the computational mesh, i.e. at $k \approx 240$. A scale-by-scale estimation of the difference between these two basic approaches can be provided by plotting the absolute deviation $|E(k) - E(k)_{\text{ref}}|$ at any computed wavenumber k for the present mesh resolution (see figure 10-right). The maximum deviation of about 10^{-4} can be considered as satisfactory for the "Euler+VF^1" case. If a higher accuracy is expected, the use of "Euler+VF^3" enables a spectacular improvement as shown by figure 10-right with a reduction by about two orders of magnitude of the deviation $|E(k) - E(k)_{\text{ref}}|$ in this case.

The capability of the viscous filtering technique is now addressed in the context of LES. For that purpose, a higher Reynolds number is considered with $Re = 10000$. The reference results are from a DNS performed at the resolution 2048^3 whereas the corresponding LES are based on ~~a~~ meshes reduced by a factor 8 or 16 in every direction with 256^3 and 128^3 nodes respectively. These two levels of mesh refinement are referred as high-resolution (HR) and low-resolution (LR). By comparison to DNS, their associated reduction of the number of degrees of freedom corresponds to a drastic decrease of the computational cost with a division by a factor of about 4000 for HR LES

and more than 65000 for LR LES. Both LES configurations can be considered as challenging in terms of SGS modelling quality, with naturally a stronger demand for LR LES.

A comparison between HR LES and DNS results is presented in figure 11 for the dissipation ε_t (left) of the kinetic energy E_k and for its spectrum $E(k)$ at $t = 14$ (right). The observation of dissipation, estimated as

$$\varepsilon_t = -dE_k/dt \tag{59}$$

by finite difference, enables a closer analysis of the differences between one result to another. The HR LES results of [4] are also included in the comparison. This ~~LES~~ calculation of reference has been performed using an implicit SVV as SGS model. For this approach, belonging to the family of implicit LES, the artificial dissipation is provided by a boost of the second derivative at small scales [23, 4] while shaping the modified wavenumber to mimic SVV. For present HR LES, the counterpart of this technique is used through a viscous filtering based on the set of coefficients (38) while using the same level of numerical dissipation with $\nu_0/\nu = 63$. Despite the non-deterministic behaviour of the flow at this Reynolds number, an excellent matching can be observed in figure 11 between present results and those from [4]. The time evolution of ε_t is in good agreement with the DNS results of reference as well as the kinetic energy spectrum $E(k)$ in the wavenumber range $0 \leq k \lesssim k_c/2$ as already reported in [4]. In the second part of the spectrum $k_c/2 \lesssim k \leq k_c$, the damping of $E(k)$ is almost identical for the reference LES [4] (referred as "Navier-Stokes LES") and for both cases "Euler+VF^1" and "Euler+VF^3" LES. This is the practical confirmation that the present viscous filtering technique can be used in the context of implicit LES as the counterpart of implicit SVV initially introduced by [23, 4] through the computation of second derivatives in the viscous term.

An attractive feature of this remarkable correspondence is that it provides a way to explicitly estimate the kinetic energy dissipation provided by the viscous filtering. As explained in [4], the estimation of ε_t can be based on the computation of second derivatives with

$$\varepsilon_t = -\nu \left\langle u_i \frac{\partial^2 u_i}{\partial x_j \partial x_j} \right\rangle \tag{60}$$

using the counterpart scheme of present viscous filtering technique. Estimations of ε_t given by (59) or (60) are virtually identical as shown in figure

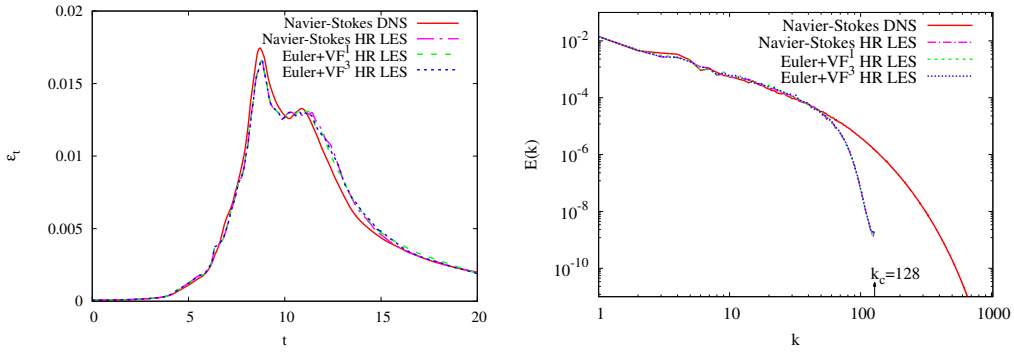

Figure 11: Left: time evolution of the kinetic energy dissipation ε_t. Right: kinetic energy spectra $E(k)$ at $t = 14$.

12-top-left where the symbols are superimposed on the curve. The availability of an accurate procedure to estimate the total dissipation ε_t (i.e. including its artificial component) is a clear advantage of the present viscous filtering technique. For instance, in the production of turbulent budgets, it is common to estimate the contribution of the artificial dissipation as the residual term assuming that budgets are perfectly balanced. With the present approach, the total dissipation can be explicitly estimated and thus this assumption is no longer required, enabling the analysis of unbalanced budget in transient turbulent states (as for the present TGV flow) or to estimate the lack of statistical convergence when a stationary state is reached.

A slight loss of quality can be observed in figure 12 (bottom) for the LR LES results. However, it is worth noting that despite the coarse mesh, the present implicit SGS modelling enable to capture the peak of dissipation with an acceptable accuracy. This means that the brutal kinetic energy cascade during the turbulent breakdown is correctly taken into account by the hyperviscous filtering, as far as the time evolution of the kinetic energy is concerned. The shape of the spectrum $E(k)$ is qualitatively similar for LR LES by comparison to HR LES (see figure 12-right-bottom) with a comparable fall from $k_c/2$ to k_c. It must be noted that the reduction of the spatial resolution requires to increase the numerical viscosity with $\nu_0/\nu = 182$ for LR LES against $\nu_0/\nu = 63$ for HR LES. These two values are predicted by the very simple Pao-like closure proposed by [4] to choose the level of artificial dissipation knowing the ratio between the LES and DNS cell sizes. Here, this ratio is 8 and 16 for HR and LR LES respectively, leading to the

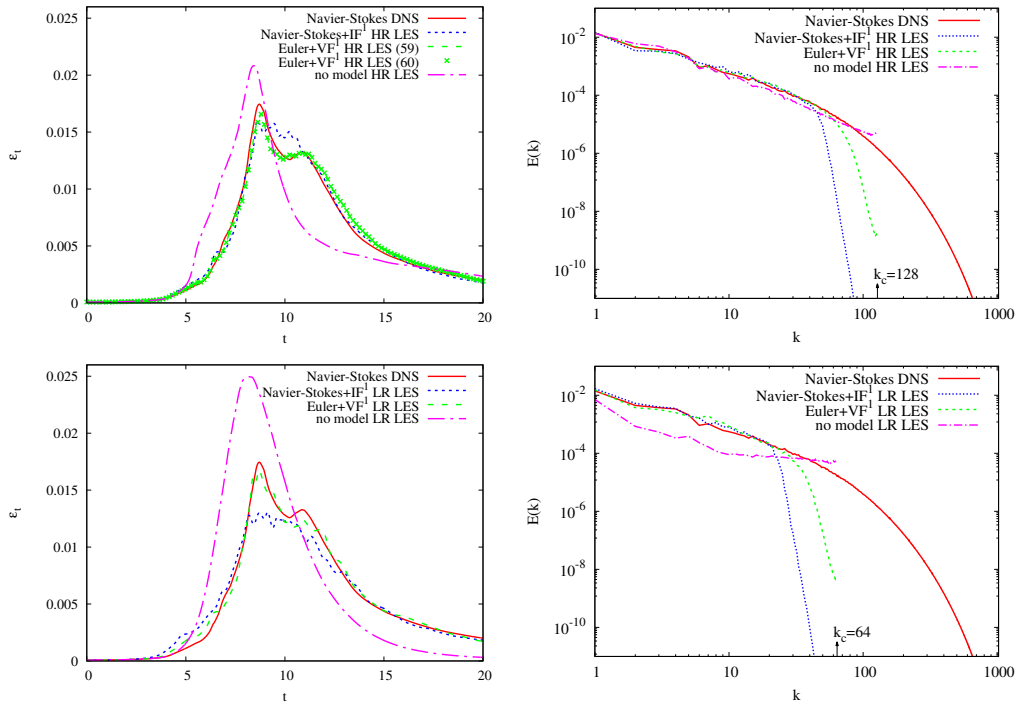

Figure 12: Left: time evolution of the kinetic energy dissipation ε_t. Right: kinetic energy spectra $E(k)$ at $t = 14$. Top: high-resolution LES. Bottom: low-resolution LES. The case "Navier-Stokes+IF^1 has been performed using the optimized 6$^{\text{th}}$-order filter of [30].

aforementioned values of ν_0/ν. The similar damping of the second part of the spectrum for HR and LR LES suggests that these predicted values are physically consistent while being transposable to the present hyperviscous filter operator.

~~Before closing this subsection, a few words can be added on~~ Let us consider now the use of filtering in combination with the explicit computation of the viscous term in Navier-Stokes equations. In that case, the filtering has to vanish at large scales, so that this approach can be referred as "Navier-Stokes+IF^1" with IF for "Inviscid Filtering". For conciseness, only the case with one filtering per time step is considered as it is commonly used in the literature. As inviscid filter, an option could be to use the set of coefficients (26) in combination with a conventional scheme for the computation of second derivatives. In practice, because this strategy would be less computationally efficient by comparison to the present viscous filtering technique while being equivalent in terms of accuracy, this specific combination is not addressed. As an example of "Navier-Stokes+IF^1" case, a filter fully removing the grid-to-grid wavelength is used with $\sigma = 1$. This is, by far, the most popular choice when the filtering solution strategy is used in DNS/LES. The filter developed by [30] is chosen for its good features of spectral vanishing at low wavenumber as illustrated in figure 2-left. The results of the corresponding calculation are presented in figure 12 for the time evolution of ε_t (left) and for the kinetic energy spectrum $E(k)$ at $t = 14$ (right). Despite the favourable scale-selective features of the filter from [30], the prediction of the total dissipation ε_t is found to be of lower quality by comparison to "Euler+VF^1" LES, the latter being less expensive thanks the dispense of second derivative computation. ~~In particular~~ For HR LES, the phase of turbulent breakdown around the secondary peak of dissipation at $t \approx 12$ is not correctly captured. Even the first peak of dissipation, corresponding to early transition, is less accurately predicted by "Navier-Stokes+IF^1" HR LES. This loss of accuracy, significantly magnified for LR LES, may be attributed to the too invasive influence of the filtering at small scales. This behaviour is well illustrated in figure 12-right by the abrupt fall of $E(k)$ due to the use of $\sigma = 1$ that corresponds to an infinite value of the numerical viscosity ν_0 because of the full removing of turbulent scales at k_c. This intrusive effect ~~of this type of filtering~~ at small scales is consistent with the equivalent SVV kernel presented in figure 2-left. A more gradual scale-selection of numerical dissipation seems to be a preferable option, with in particular a finite value for ν_0. ~~For a choice of ν_0/ν based on physical considerations, the reader is~~

~~referred to [4].~~

A fundamental issue is the evaluation of the actual role of the artificial dissipation while relating it to what can be expected from a SGS model. The simplest way to assess the activity of any SGS modelling, whether implicit or explicit, is to switch off the model and then observe the consequences on the results. This type of calculation can be referred as "no model" LES. For the present approach, no model means that no filtering is applied while using a conventional scheme, free from any artificial dissipation, for the computation of second derivatives. For both HR and LR LES, the lack of regularisation is found to lead to very inaccurate results. The loss of accuracy can be directly observed on the time evolution of the kinetic energy, with in particular a clear overestimation of the dissipation (see figure 12-left). As expected, no model LR LES results are worse than their HR LES counterparts. An examination of instantaneous solutions (not shown) reveals that no model LES solutions are subject to small-scale oscillations. These spurious oscillations tend to magnify the viscous friction, explaining the paradox that the lack of artificial dissipation leads to an overdissipative behaviour. The signature of these unphysical oscillations on the spectrum $E(k)$ can be observed in figure 12-right as a pile-up of kinetic energy in the spectral range $k_c/2 \lesssim k \leq k_c$, especially for LR LES for which $E(k)$ becomes almost flat in an extended range of k, indicating the establishment of an unphysical white noise which can be seen as a partial thermalization of the flow.

Another way to assess the role of the artificial dissipation is to estimate its relative contribution to the total dissipation. Here, we propose to make indirectly this estimation by computing first the viscous large-scale dissipation ε_{LS}. Then, in agreement with the standard definitions of SGS modelling, the SGS dissipation ε_{SGS} can be defined as $\varepsilon_{SGS} = \varepsilon_t - \varepsilon_{LS}$ where ε_t is the total dissipation provided by the hyperviscous filtering as a sum of its artificial (equated with SGS contribution) and viscous (equated with large-scale contribution) parts. A reasonable choice to estimate ε_{LS} is to use a standard second derivative scheme free from extra dissipation to compute the right-hand side of (60). Because these estimations are based on LES results, they can be referred as *a posteriori* analysis. To check their reliability, an *a priori* analysis based on raw and filtered DNS data has also been performed. For that purpose, the same methodology as in [38] has been carried out, enabling to provide an *a priori* estimation of both ε_{LS} and ε_{SGS}. The filtered DNS data are generated consistently with the numerical dissipation through the use of a simplified spectral closure as explained in [4]. For both HR and LR

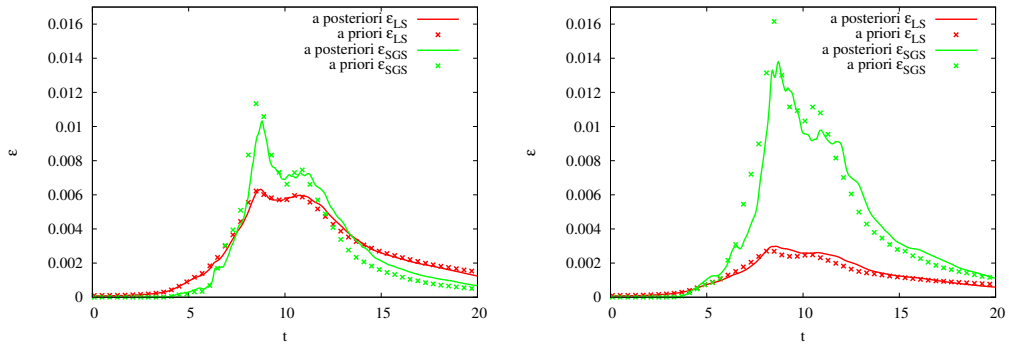

Figure 13: Time evolution of the viscous large-scale kinetic energy dissipation ε_{LS} and of its SGS counterpart ε_{SGS} with $\varepsilon_t = \varepsilon_{LS} + \varepsilon_{SGS}$. Left: high-resolution LES. Right: low-resolution LES.

LES, a good agreement is obtained between these *a posteriori* and *a priori* estimations as shown in figure 13. Because this agreement is obtained without any constant adjustment, it can be considered as successful. Both *a priori* and *a posteriori* analyses confirm that even HR LES is quite challenging in the sense that ε_{SGS} can correspond, during the turbulent breakdown, to more than 60% of ε_t. For LR LES, this relative contribution of the SGS dissipation to the total dissipation can reach more than 80%. This is a clear confirmation, consistent with the no model results, that the present type of implicit SGS modelling plays a major role.

To conclude this subsection, let us compare the computational efficiency of "Euler+VF" and "Navier-Stokes" DNS/LES. In the code Incompact3d, the Euler (i.e. the convection and pressure terms) and viscous parts require the computation of 24 first and 9 second derivatives respectively. Removing the viscous term while applying a viscous filtering once every time step (referred here as "Euler+VF^1") simply consist in the substitution of these 9 second derivatives by the 9 one-dimensional filter operations (i.e. one by direction) without impacting the computational cost. If the more time accurate strategy "Euler+VF^3" is adopted, the extra application of 18 one-dimensional filters results in an increase of about +56% of the computational cost. Viewed in this perspective, the viscous filtering technique does not present any advantage by comparison to the traditional solving of Navier-Stokes equations. It can only be said that the "Euler+VF^1" approach reduces the computational cost by about −21% by comparison to the conventional

"Navier-Stokes+IF[1]" strategy thanks to the dispense of computation of the 9 second derivatives in the viscous term.

Because the strongest time step restriction comes from the CFL condition in the present DNS/LES of TGV, there is no interest in using a viscous filtering as a way to relax the viscous stability condition. In the next subsection, a more challenging situation is addressed where the stability limit is mainly dictated by the time integration of the viscous term.

7.2. Turbulent pipe flow

As a second computational configuration, DNS of a turbulent pipe flow at low and high Reynolds numbers are addressed. Again, the code Incompact3d is used with the solving of an extra governing equation for a passive scalar in order to provide heat transfer predictions. The computational domain $L_x \times L_y \times L_z$ is discretized using a regular Cartesian mesh of $n_x \times n_y \times n_z$ nodes despite the cylindrical geometry which is modelled thanks to an immersed boundary method customised for Incompact3d [39]. This computational configuration enables the imposition of periodic boundary conditions in the streamwise z as well as in the transverse x, y directions.

The physical boundary conditions imposed at the pipe wall are no-slip for the velocity and mixed-type for the temperature [40]. Numerically, both can be treated as Dirichlet-type boundary conditions. Defining the Reynolds number on the bulk velocity U_b and the pipe diameter D, its two addressed values are $Re = (5300, 37700)$ at the same Prandtl number $Pr = 0.71$. For the Reynolds numbers based on the friction velocity u_τ, the two related nominal values are $Re_\tau = 180, 1000$. The streamwise length of the computational domain is the same for both Reynolds numbers with $L_z = 12.5D$; concerning the transverse dimensions, at $Re = 5300$ a slightly larger size is used with $L_x = L_y = 1.28D$ against $L_x = L_y = 1.12D$ at $Re = 37700$. This adjustment of the computational domain enables us to ensure a minimum number of nodes inside the solid region that corresponds to the pipe wall thickness t_w with $t_w \approx 0.075D$ at $Re = 5300$ and $t_w \approx 0.016D$ at $Re = 37700$. The computational mesh is based on $n_x \times n_y \times n_z = 256 \times 256 \times 640$ and $n_x \times n_y \times n_z = 768 \times 768 \times 1920$ nodes for the low and high Reynolds number respectively. For a schematic view of the computational configuration, see figure 14 where the principle of the solution reconstruction inside the immersed boundary is illustrated [39].

Expressed in wall units, the related cell sizes are $\Delta z^+ = (7, 13)$ and $\Delta x^+ = \Delta y^+ = (1.8, 2.9)$ at $Re = (5300, 37700)$. These spatial resolutions can

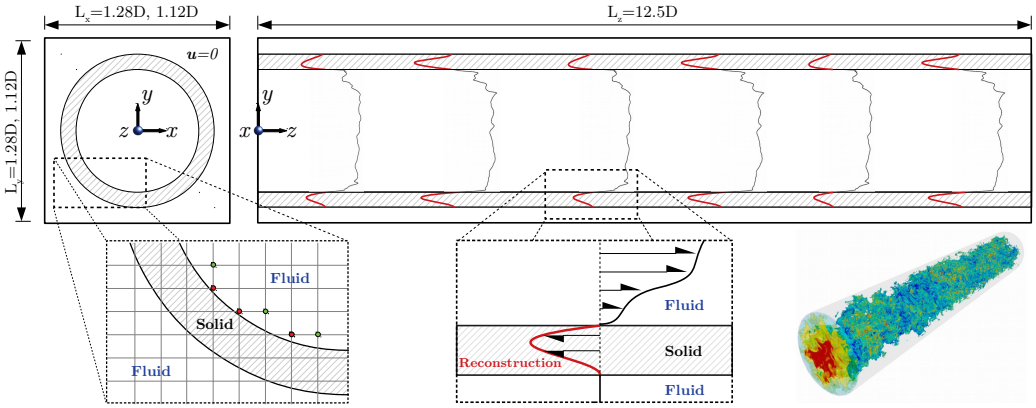

Figure 14: Schematic view of the computational configuration of the pipe flow. Hatched zone indicates the solid region modelled by a customised immersed boundary based on solution reconstruction inside the solid [39].

be considered as fine except in the near-wall region for $\Delta x^+ - \Delta y^+$, especially for the high Reynolds case. However, it has been shown by [41, 42] that this type of Cartesian mesh can provide basic turbulent statistics reaching the DNS accuracy. This is why we refer to DNS in this subsection, as a reliable computational configuration to assess the present viscous filtering technique while showing its major advantage in terms of computational efficiency.

The principle of comparison is the same as in the previous section. The reference data are from DNS based on the conventional way to compute the viscous term in the governing equations, referred here as "Navier-Stokes" DNS. The original data are obtained by the strategy "Euler+VF" DNS, namely through the solving of Euler equations while applying the viscous filter once ("Euler+VF^1" DNS) or three times ("Euler+VF^3" DNS) per time step. The viscous filter is given by (1,36) as the counterpart of the second derivative scheme from [23] on which are based the reference "Navier-Stokes" DNS. As in the DNS of TGV presented in the previous subsection, aliasing errors are controlled using a moderate value of the numerical viscosity with $\nu_0/\nu = 3$. For the present pipe flow DNS, this artificial dissipation significantly improves the results contrary to the TGV flow for which it is of secondary importance.

It is important to stress that, unlike the previous subsection, the present comparisons between "Navier-Stokes" DNS and "Euler+VF" DNS are not based on the same time step. For the "Navier-Stokes" DNS, the more severe

restriction on Δt comes from the AB3 Fourier condition (45) which reads $F < 0.0138$ for $\nu_0/\nu = 3$.

In the present computational flow configuration, based on immersed boundary condition, the correct definition of F is not obvious. Firstly, because of the Prandtl number less than unity, the most restrictive condition comes from the diffusion term in the temperature equation so that it is more convenient to define the Fourier number using the thermal diffusivity α instead of the viscosity ν. Secondly, concerning the reference length in F, an option could be to simply consider the smallest cell size given by Δx or Δy. From this definition of F, the maximum time step ensuring numerical stability should be $U_b \Delta t/D \approx (1.30\,10^{-3}, 8.87\,10^{-4})$ for $Re = (5300, 37700)$. In practice, for the present "Navier-Stokes" DNS, these maximum values cannot be approached without losing numerical stability when an immersed boundary method is used. These maximum time steps have been therefore determined empirically. For the two configurations addressed here, the obtained values are $U_b \Delta t/D \approx (4\,10^{-4}, 2\,10^{-4})$ for $Re = (5300, 37700)$, about 25%-30% of their reference values predicted by numerical stability analysis, corresponding to a strong reduction of the computational efficiency.

One reason of this difficulty lies in the mesh node distribution disconnected from the wall geometry. This feature, which is a strength of immersed boundary methods, imposes the computation of the solution on mesh nodes very close to the wall, namely at a clearly smaller distance than the mesh size. Figure 14 illustrates this situation with a red mark for these very near-wall nodes by contrast to the others marked in green. This irregular mesh topology in terms of wall distance suggests that Δx may not be the correct length scale to estimate the maximum Fourier number. To the best of the authors' knowledge, a numerical stability analysis of this problem, inherent to the immersed boundary method, is not documented in the literature. Here, we presume that, when expressing the Fourier condition, its reference length should be corrected in order to take into account the occurrence of mesh nodes very close to the wall. This corrected cell size Δc can be estimated from the empirical determination of the maximum numerically stable Δt. Based on the 25%-30% reduction of the time step previously mentioned, we get the crude estimation $\Delta c \approx 0.5 \Delta x$ which can be seen, in first approximation, as a median value of the distance of the closest mesh nodes from the wall.

The crucial advantage of the present viscous filtering technique is the strong relaxation on the Fourier condition with $F < 4.12$ for the present

scheme (1,36) as already mentioned in section 6. For the present DNS, this condition is clearly less restrictive on the time step than the CFL condition which enables the use of a time step $(6, 3.5)$ times larger in "Euler+VF" DNS by comparison to "Navier-Stokes" DNS for the case $Re = (5300, 37700)$ respectively. Naturally, the point is to ensure that the resulting computational saving is not against accuracy. The following comparisons address this key issue.

Profiles of mean velocity, turbulent kinetic energy, mean temperature and temperature variance are presented in figure 15 at $Re = 5300$ for "Navier-Stokes" DNS, "Euler+VF^1" DNS and "Euler+VF^3" DNS. Present turbulent statistics are estimated through a smoothed projection from the Cartesian mesh to the cylindrical coordinates (r, θ) with an average in time and in the azimuthal direction θ (see [41] for more details on the data projection technique). The DNS data of [43] are also included for reference. For all of these quantities, an excellent agreement can be observed. The very small discrepancies are within the statistical convergence uncertainty. As in the previous subsection, the difference between "Euler+VF^1" DNS and "Euler+VF^3" DNS is found to be insignificant, making questionable the practical interest of the extra cost of +56% due to the two additional filtering applications per time step. This conclusion is not unexpected: it is well-known that because of time-scale ratio between convection and diffusion processes, the viscous term can be integrated in time using a scheme of lower accuracy by comparison to the convection term. By accepting the negligible loss of time accuracy of "Euler+VF^1" DNS, it can be concluded that the present viscous filtering strategy reduces by -83% the computational cost by comparison to an explicit time integration of the viscous term. For "Euler+VF^3" DNS, the computational saving is only -74% which is nonetheless very satisfactory.

The advantage of viscous filtering can be even more spectacular at low Prandtl number Pr. This can be particularly useful in applications involving liquid metals, such as advanced cooling devices, in which the prediction by DNS/LES of heat-transfer in turbulent flows of low-Pr fluids is necessary for design purposes. Because of the corresponding high value of the thermal diffusivity α, an explicit time integration of the viscous term becomes extremely penalizing requiring the use of a very small time step in order to ensure the Fourier condition. With the present viscous filtering technique, low-Pr fluids can be addressed without any extra-cost. To illustrate this capability, a case at $Pr = 0.025$ has been considered by DNS at $Re = 5300$. At this high level of diffusion, there is no need to apply any artificial dis-

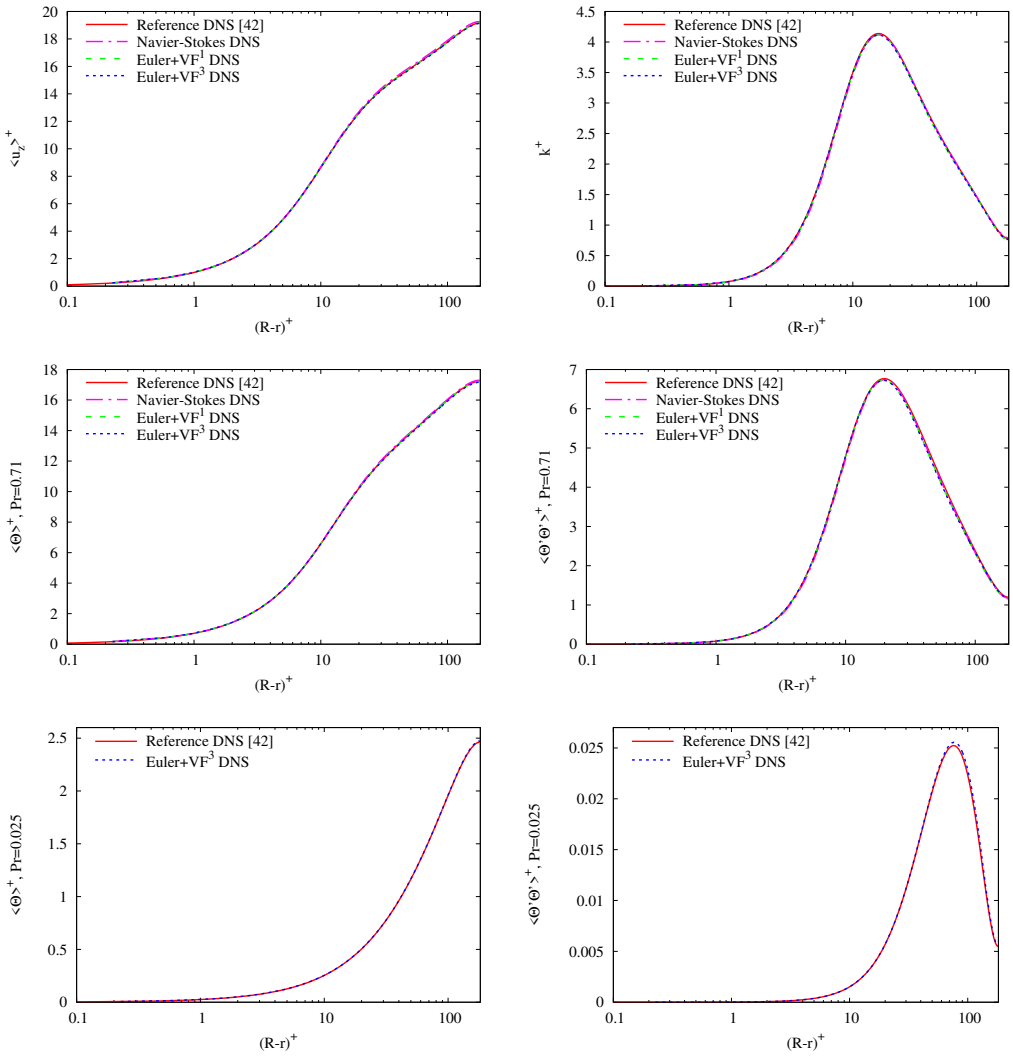

Figure 15: Profiles of mean velocity $\langle u_z \rangle$, turbulent kinetic energy k, mean temperature $\langle \Theta \rangle$ and temperature variance $\langle \Theta' \Theta' \rangle$ at $Re = 5300$. Temperature statistics at $Pr = 0.71$ (middle) and $Pr = 0.025$ (bottom).

sipation for the temperature equation ($\nu_0 = 0$). Despite the corresponding less restrictive Fourier condition $F < 0.00425$, the high value of the diffusivity would make too expensive a "Navier-Stokes" DNS. On the contrary, an "Euler+VF" DNS without changing the time step can be easily performed. A comparison of the resulting temperature statistics with the reference data of [43] is presented in figure 15-bottom. Again, an excellent agreement is obtained. The same computation by "Navier-Stokes" DNS would have required a time step 30 times smaller, leading to a computational saving of -95% for the "Euler+VF^3" DNS.

To confirm the good behaviour of the present viscous filtering approach, a more demanding computational configuration at $Re = 37700$ is now considered. As already mentioned, expressed in wall units, the spatial resolution is marginal, especially in the near-wall region. In such a situation, the use of artificial dissipation is crucial to compensate the small fraction of viscous dissipation missed due to the too coarse mesh to fully capture the Kolmogorov scale. At this Reynolds number, successful turbulent velocity statistics have been obtained by [44] with the same computational configuration using the conventional strategy "Navier-Stokes" DNS. In figure 16, turbulent statistics with the present "Euler+VF^3" DNS approach are compared to the DNS of [45] for velocity and to the well-resolved LES of [43] for temperature[4]. Despite the marginal resolution for this high Reynolds number case, a good overall agreement can be observed. The ability of "Euler+VF^3" DNS to faithfully reproduce the reference results despite the use of a 3.5 times larger time step by comparison to "Navier-Stokes" DNS shows that the present viscous filtering approach is not only attractive for low Reynolds turbulence. It leads to a reduction of about -55% that can be extended to -71% if the simpler and slightly less accurate "Euler+VF^1" DNS strategy is used. In conclusion, as a generic, stable, efficient and accurate method, the "Euler+VF" DNS seems to be a convenient technique for solving the Navier-Stokes equations.

8. Conclusion and discussion

In this study, a new approach of spatial filtering is proposed for solving the governing equations of fluid mechanics. The general framework of this approach is the concept of solution filtering which consist in the application

[4] As [43], we refer to LES, but it must be noted that, thanks to the very fine mesh used, the accuracy of this calculation is very close to DNS.

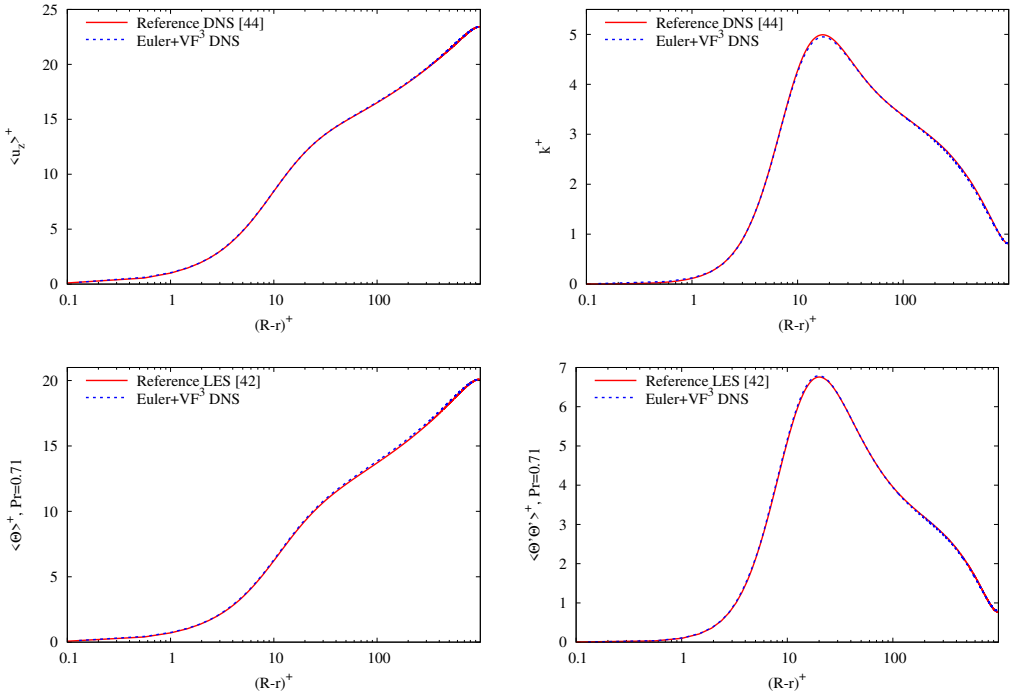

Figure 16: Profiles of mean velocity $\langle u_z \rangle$, turbulent kinetic energy k, mean temperature $\langle \Theta \rangle$ and temperature variance $\langle \Theta' \Theta' \rangle$ at $Re = 37700$. Temperature statistics at $Pr = 0.71$.

of a spatial filter operator every step of the time advancement. The method is developed in the context of finite-difference schemes as a simple spatially discrete integrating factor commonly used in spectral Fourier methods for computational fluid dynamics [33, 34].

First, the guiding principles of the solution filtering technique have been discussed while clearly exhibiting the flexibility of the method through the adjustment of the scheme coefficients. In this preliminary part, the equivalence between solution filtering and spectral vanishing viscosity is shown. To the authors' knowledge, this is the first time that this link is clearly established. Thanks to the simple formalism related to this connection, the consequences of using a fixed filter are discussed as well as the physical anomaly that consists in fully removing the grid-to-grid wavelength that must be associated to the application of an infinite artificial viscosity at this scale. Another issue raised by the use of a fixed filter scheme is the lack of time consistency. As a very simple remedy to these drawbacks, it is suggested to make dependent the scheme coefficients on the time step Δt. It leads to a first family of flexible filters that can be shaped to mimic a generic spectral vanishing viscosity while controlling the level of artificial dissipation at small scales through the parameter ν_0 referred as numerical viscosity. As nondimensional parameters to represent Δt and ν_0 in the scheme coefficients, the Fourier number F and the ratio ν_0/ν are introduced. Because of the spectral vanishing behaviour of these finite-difference operators, they can be referred as inviscid filters (i.e. virtually free from any significant dissipation at large scales).

Then, the principle of modifying the filter scheme coefficients is extended in order to incorporate both the molecular and artificial dissipations in one single operator. The development of this new family of filter schemes is performed in the Fourier space to make easier the establishment of relation orders between the scheme coefficients. This leads to the new concept of viscous filtering while keeping the initial philosophy to apply the filter on the solution every time step. Various sets of scheme coefficients are provided on the basis of 8^{th}-order accuracy in space. These coefficients are a function of F and ν_0/ν. Each viscous filter operator is connected to its counterpart as a differentiation operator to compute a second derivative. Based on this link, it can be shown that the actual order of accuracy of the viscous filter is reduced by two levels by comparison to its formal order, leading to 6^{th}-order for the family developed in this study. The same link shows that the solution provided by the viscous filter is a 1^{st}-order approximation in time of its counterpart obtained using a second derivative scheme with an exact time

integration (see Appendix A). Spatial convergence test confirms the 6^{th}-order accuracy of the developed viscous filter scheme. Temporal convergence shows that despite the 1^{st}-order previously mentioned, because of the entanglement between spatial and time errors, the viscous filtering is always more accurate in time than an Adams-Bashforth scheme of 3^{rd}-order accuracy. By comparison to this explicit time advancement scheme, it can be observed that the present viscous filtering strategy is much more robust in terms of numerical stability, with a spectacular relaxation of the Fourier condition.

The accuracy as well as the numerical stability features of the viscous filtering technique are recovered for challenging DNS/LES of two academic flows. For the Taylor-Green Vortex problem, the study of a deterministic regime at low Reynolds number has enabled very accurate comparisons between a conventional solving of Navier-Stokes equations (based on the explicit computation of the viscous term) and the present new viscous filtering approach. A higher Reynolds number is also considered by LES to show the capability of the method as an implicit subgrid-scale model. As a generic wall-turbulence problem, the turbulent pipe flow has been calculated by DNS while considering heat transfer. The treatment of this cylindrical geometry with an immersed boundary method and a Cartesian mesh has enabled us to assess the method as a more general approach compatible with complex geometry. Successful results are obtained in the sense that the viscous filtering strategy can reach an excellent accuracy while reducing drastically the computational cost thanks to the use of large time steps. This facility is allowed by the very favourable numerical stability of the time advancement provided by viscous filtering. In particular, this is a definitive advantage in the context of immersed boundary method, low Reynolds and/or low Prandtl turbulent flows.

The present viscous filtering method can be seen as an alternative to implicit time integration of the viscous term which is very popular in the context of DNS/LES of wall turbulence when unconditional stability is expected, enabling to deal with any value of the Fourier number F. For the present method, the conditional stability is not removed but its restriction is so relaxed that it is close to unconditional stability. By comparison to implicit methods, the treatment of the viscous influence as a filtering process offers advantages in terms of flexibility (control of the molecular/artificial dissipations) and efficiency (no operator inversion required). It is also extremely easy to code in the sense that any finite-difference routine can be straightforwardly adapted through the simple changing of the scheme coefficients. This

is an almost "zero development" method contrary to the implementation of an implicit time integration, especially in a three-dimensional context. Here, because the filtering is explicit in time, the filter operators can be applied sequentially in every direction without any difficulty in terms of coding.

Further work is required to extend the validity of the viscous filtering approach. First, one-sided viscous filter schemes need to be developed for the imposition of Dirichlet and Neumann boundary conditions. A slightly more delicate step is to generalize the viscous filtering for a non-regular computational mesh. The use of a mapping technique may be the most straightforward way to take this step but other methods, possibly more efficient, are probably feasible.

A few words can be added on the anisotropic and inhomogeneous application of the viscous filtering through the choice of ν_0/ν related to the artificial dissipation. Technically, the use of a different value of ν_0/ν depending on the spatial direction is straightforward in the sense that the present filtering strategy is based on one-dimensional finite-difference operators. Then, if there are physical reasons for an anisotropic application of the artificial dissipation, it can be done easily. In the same way, its inhomogeneous application is technically feasible by enabling spatial variation of ν_0/ν for the computation of the coefficients of the finite-difference filter scheme at every mesh node. Another option is to use two sets of constant coefficients, one with $\nu_0/\nu = 0$ and another with a high value of ν_0/ν. Then, a local switch between the two operators (one free from artificial viscosity and another one highly dissipative at small scale) can be performed. This second option has been investigated by [46] for the boosted second derivative which is the counterpart of the present viscous filtering. The simplicity and efficiency of this approach, called Adaptive Numerical Viscosity (ANV), is clearly shown in this study. To summarize, there is no technical barrier for an anisotropic and inhomogeneous application of the artificial dissipation embedded in the present viscous filtering technique.

A more fundamental question is related to the purpose of an anisotropic and inhomogeneous application of numerical dissipation. In terms of physical scales, the use of the same value of ν_0/ν in the three spatial directions does not mean than the artificial dissipation is isotropic. It is only true if the computational mesh itself is isotropic. For instance, in the turbulent pipe flow DNS presented in section 7.2, the use of non-cubic cells, with an aspect ratio of about 4, leads to an anisotropic numerical dissipation despite the same value $\nu_0/\nu = 3$ used in the three spatial directions. For a regular

and Cartesian computational mesh, directional values of ν_0/ν would only be useful to compensate a potential mismatch between physics and numerics. In other words, instead of imposing anisotropy on the numerical viscosity, a preferable option would be to adapt the computational mesh. A similar idea can be advocated for the use of inhomogeneous numerical dissipation that should be first reflected by the mesh design. This corresponds to the general recommendation of [4] (see concluding section) who suggest to adapt the LES mesh on its corresponding DNS counterpart using a constant and isotropic derefinement factor everywhere, this choice making meaningful the use of a constant numerical viscosity. This recommendation can be extended to the present viscous filtering, at least in first intention.

A common motivation for spatially varying subgrid-scale viscosity is also the treatment of wall turbulence, with typically a damping of the model activity in the near-wall region. This approach has been investigated by [46] using their technique of Adaptive Numerical Viscosity for LES of turbulent plane channel flow up to very high Reynolds numbers. Their conclusion was that a local adaptation of ν_0/ν was not really needed, even for the most demanding computational configuration addressed. This conclusion is consistent with our pipe flow LES reported in [44] and based on the use of boosted second derivatives. In this previous study, it has been shown that good turbulent statistics can be obtained while using a constant value for ν_0/ν. This easiness probably comes from the high scale-selectivity of the numerical dissipation which is weakly intrusive on the largest scale dynamics.

Naturally, in a perspective of advanced subgrid-scale modelling, the spatial variation of ν_0/ν may be a physically meaningful option. For instance, to deal with the unsteady and inhomogeneous component of non-equilibrium turbulent cascade [47], the opportunity of controlling locally and instantaneously the strength of the kinetic energy transfer may be an attractive feature. Hence, scaling of the artificial dissipation, related to the choice of ν_0/ν, can be guided by physical considerations on the kinetic energy transfer ~~between~~ from large ~~and~~ to subgrid scales. Naturally, because the present approach is purely dissipative, no backscatter phenomenon can be handled in this way. However, in complement to the simple spectral closure of [4] only valid for isotropic turbulence at equilibrium, as a tool for *a priori* estimation of ν_0/ν, a more dynamic evaluation of this parameter, as in the adaptive filtering of [12, 14], may be an interesting option~~, requiring to recompute the filter scheme coefficients every time step~~.

~~The scaling of the artificial dissipation for LES, related to the choice of~~

~~ν_0/ν, could also be more guided by physical considerations on the kinetic energy transfer between large and subgrid scales. In complement to the simple spectral closure of [4] only valid for isotropic turbulence at equilibrium, as a tool for a priori estimation of ν_0/ν, a more dynamic evaluation of this parameter, as in the adaptive filtering of [12][14], may be an interesting option, requiring to recompute the filter scheme coefficients every time step.~~

The extension of the concept of viscous filtering may also be adapted to more sophisticated spectral/hp element approaches [48, 49], as a contribution to the development of implicit LES in highly accurate DNS/LES solvers [50, 51]. In this demanding context, the present combination of high-order finite-difference schemes with an immersed boundary method can be seen as a simple and efficient strategy which is reinforced by this particular way to model viscous effects.

Appendix A. Connection between viscous filter and second derivative schemes at small Fourier number

In this appendix, the asymptotic behaviour of the viscous filter when $F \to 0$ is examined. It will be shown that the modified wavenumber given by (33) can be seen as a 1$^{\text{st}}$-order $O(\Delta F)$ approximation of the modified wavenumber of a counterpart second derivative scheme written in the form

$$\begin{aligned} \alpha f''_{i-1} + f''_i + \alpha f''_{i+1} = a\frac{f_i}{\Delta x^2} &+ b\frac{f_{i-1}+f_{i+1}}{2\Delta x^2} + c\frac{f_{i-2}+f_{i+2}}{2\Delta x^2} \\ &+ d\frac{f_{i-3}+f_{i+3}}{2\Delta x^2} + e\frac{f_{i-4}+f_{i+4}}{2\Delta x^2} \end{aligned} \tag{A.1}$$

with its associated modified wavenumber

$$k''\Delta x^2 = -\frac{a + b\cos(k\Delta x) + c\cos(2k\Delta x) + d\cos(3k\Delta x) + e\cos(4k\Delta x)}{1 + 2\alpha\cos(k\Delta x)} \tag{A.2}$$

where f''_i is an approximation of the second derivative $f''(x_i)$ at the node x_i. Here, to make easier the connection between this scheme and the viscous filter, the adopted form mimics the generic form of a filter scheme without any loss of generality in the framework of centred schemes based on a given

stencil. For this scheme, the order conditions can be easily obtained with

$$\begin{aligned} 0 &= a+b+c+d+e && (\Delta x^0) \\ 2+4\alpha &= b+4c+9d+16e && (\Delta x^2) \\ 24\alpha &= b+16c+81d+256e && (\Delta x^4) \\ 60\alpha &= b+64c+729d+4096e && (\Delta x^6) \end{aligned} \tag{A.3}$$

This set of conditions has similarities with the order conditions (31) of the viscous filter which can also be written as

$$\begin{aligned} 0 &= \frac{a_f-1}{F}+\frac{b_f-2\alpha_f}{F}+\frac{c_f}{F}+\frac{d_f}{F}+\frac{e_f}{F} && (\Delta x^2) \\ 2+4\alpha_f &= \frac{b_f-2\alpha_f}{F}+4\frac{c_f}{F}+9\frac{d_f}{F}+16\frac{e_f}{F} && (\Delta x^4) \\ 12F(1+2\alpha_f)+24\alpha_f &= \frac{b_f-2\alpha_f}{F}+16\frac{c_f}{F}+81\frac{d_f}{F}+256\frac{e_f}{F} && (\Delta x^6) \\ 120F^2(1+2\alpha_f)+360F\alpha_f+60\alpha_f &= \frac{b_f-2\alpha_f}{F}+64\frac{c_f}{F}+729\frac{d_f}{F}+4096\frac{e_f}{F} && (\Delta x^8) \end{aligned} \tag{A.4}$$

In particular, it can be concluded that the set of coefficients

$$\left(\alpha_f, \frac{a_f-1}{F}, \frac{b_f-2\alpha_f}{F}, \frac{c_f}{F}, \frac{d_f}{F}, \frac{e_f}{F}\right) \tag{A.5}$$

is a $O(\Delta F)$ approximation of the set of coefficient (α, a, b, c, d, e).

The logarithmic term $\ln T$ in (33) can be written and approximated as

$$\ln\left[1+F\frac{\frac{a_f-1}{F}+\frac{b_f-2\alpha_f}{F}\cos(k\Delta x)+\frac{c_f}{F}\cos(2k\Delta x)+\frac{d_f}{F}\cos(3k\Delta x)+\frac{e_f}{F}\cos(4k\Delta x)}{1+2\alpha_f\cos(k\Delta x)}\right] = F\frac{\frac{a_f-1}{F}+\frac{b_f-2\alpha_f}{F}\cos(k\Delta x)+\frac{c_f}{F}\cos(2k\Delta x)+\frac{d_f}{F}\cos(3k\Delta x)+\frac{e_f}{F}\cos(4k\Delta x)}{1+2\alpha_f\cos(k\Delta x)}+O(\Delta F^2) \tag{A.6}$$

Then, using (33), the corresponding approximated modified wavenumber is

$$\begin{aligned} k''\Delta x^2 &= -\frac{\frac{a_f-1}{F}+\frac{b_f-2\alpha_f}{F}\cos(k\Delta x)+\frac{c_f}{F}\cos(2k\Delta x)+\frac{d_f}{F}\cos(3k\Delta x)+\frac{e_f}{F}\cos(4k\Delta x)}{1+2\alpha_f\cos(k\Delta x)} \\ &\quad +O(\Delta F) \end{aligned} \tag{A.7}$$

as the counterpart of (A.2) for a second derivative scheme where the set of coefficients (A.5) is recovered to replace (α, a, b, c, d, e).

These developments show that the present viscous filter corresponds to a second derivative which behaves asymptotically as a conventional second derivative finite-difference scheme when $F \to 0$. The scaling in F means that this approximation is 1^{st}-order accurate in time while leading to a reduction of 2 for the spatial order of accuracy. It explains why the present 8^{th}-order filter formulation can only provide 6^{th}-order accuracy.

Acknowledgement

This work was granted access to the HPC resources of TGCC/CINES under the allocation A0052A07624 made by GENCI. The authors are indebted to Damien Biau for his insightful remarks on the topics considered here.

References

[1] B. Geurts, Elements of direct and large-eddy simulation, Edwards, 2004.

[2] P. Sagaut, Large eddy simulation of incompressible flow: an introduction, 2nd Edition, Springer-Verlag, 2005.

[3] M. Lesieur, O. Métais, P. Comte, Large-eddy simulation of turbulence, Cambridge University Press, 2005.

[4] T. Dairay, E. Lamballais, S. Laizet, C. Vassilicos, Numerical dissipation vs. subgrid-scale modelling for large eddy simulation, J. Comp. Phys. 337 (2017) 252–274.

[5] A. K. Edoh, N. L. Mundis, C. L. Merkle, A. R. Karagozian, V. Sankaran, Comparison of artificial-dissipation and solution-filtering stabilization schemes for time-accurate simulations, J. Comp. Phys. 375 (2018) 1424–1450.

[6] J. Berland, P. Lafon, F. Daude, F. Crouzet, C. Bogey, C. Bailly, Filter shape dependence and effective scale separation in large-eddy simulations based on relaxation filtering, Computers and Fluids 47 (2014) 65–74.

[7] F. Kremer, C. Bogey, Large-eddy simulation of turbulent channel flow using relaxation filtering: Resolution requirement and Reynolds number effects, Computers and Fluids 116 (2015) 17–28.

[8] T. Lund, The use of explicit filters in large eddy simulation, Computers & Mathematics with Applications 46 (4) (2003) 603–616.

[9] Klein, An attempt to assess the quality of large eddy simulations in the context of implicit filtering, Flow Turb. Combust. 75 (2005) 131–147.

[10] S. Bose, P. Moin, D. You, Grid-independent large-eddy simulation using explicit filtering, Phys. Fluids 22 (105103) (2010) 1–1.

[11] C. Bogey, C. Bailly, Large eddy simulations of transitional round jets: influence of the Reynolds number on flow development and energy dissipation, Phys. Fluids 18 (6) (2006) 1–14.

[12] T. Tantikul, J. A. Domaradzki, Large eddy simulations using truncated Navier-Stokes equations with the automatic filtering criterion, J. Turbulence 11 (21) (2010) 1–24.

[13] D. Fauconnier, C. Bogey, E. Dick, On the performance of relaxation filtering for large-eddy simulation, J. Turbulence 14 (1) (2013) 22–49.

[14] G. Sun, J. A. Domaradzki, Implicit LES using adaptive filtering, J. Comp. Phys. 359 (2018) 380–408.

[15] M. R. Visbal, D. P. Rizzetta, Large-eddy simulation on curvilinear grids using compact differencing and filtering schemes, J. Fluids Engine. 124 (4) (2002) 836–847.

[16] D. P. Rizzetta, M. R. Visbal, G. A. Blaisdell, A time-implicit high-order compact differencing and filtering scheme for large-eddy simulation, Int. J. Numer. Methods Fluids 42 (6) (2003) 665–693.

[17] C. Bogey, C. Bailly, Computation of a high Reynolds number jet and its radiated noise using large eddy simulation based on explicit filtering, Computers and Fluids 35 (2006) 1344–1358.

[18] C. Bogey, C. Bailly, Turbulence and energy budget in a self-preserving round jet: direct evaluation using large eddy simulation, J. Fluid Mech. 627 (2009) 129–160.

[19] G. Aubard, P. S. Volpiani, X. Gloerfelt, J.-C. Robinet, Comparison of subgrid-scale viscosity models and selective filtering strategy for large-eddy simulations, Flow Turb. Combust. 91 (3) (2013) 497–518.

[20] A. K. Edoh, N. L. Mundis, A. R. Karagozian, V. Sankaran, Balancing aspects of numerical dissipation, dispersion, and aliasing in time-accurate simulations, Int. J. Numer. Methods Fluids In press (2020) 1–22.

[21] J. Boris, F. Grinstein, E. Oran, R. Kolbe, New insights into large-eddy simulation, Fluid Dynamics Research 10 (1992) 199–228.

[22] F. F. Grinstein, L. G. Margolin, W. J. Rider (Eds.), Implicit Large Eddy Simulation: Computing Turbulent Fluid Dynamics, Cambridge Univ. Press., 2007.

[23] E. Lamballais, V. Fortuné, S. Laizet, Straightforward high-order numerical dissipation via the viscous term for direct and large eddy simulation, J. Comp. Phys. 230 (2011) 3270–3275.

[24] E. Tadmor, Convergence of spectral methods for nonlinear conservation laws, SIAM J. Numer. Anal. 26 (1) (1989) 1–30.

[25] Y. Maday, E. Tadmor, Analysis of the spectral vanishing viscosity method for periodic conservation laws, SIAM J. Numer. Anal. 26 (4) (1989) 854–870.

[26] G.-S. Karamanos, G. E. Karniadakis, A spectral vanishing viscosity method for large-eddy simulations, J. Comp. Phys. 163 (11) (2000) 22–50.

[27] R. Pasquetti, Spectral vanishing viscosity method for large-eddy simulation of turbulent flows, Journal of Scientific Computing 27 (1–3) (2006) 365–375.

[28] S. K. Lele, Compact finite difference schemes with spectral-like resolution, J. Comp. Phys. 103 (1992) 16–42.

[29] J. W. Kim, R. D. Sandberg, Efficient parallel computing with a compact finite difference scheme, Computers and Fluids 58 (2012) 70–87.

[30] C. Bogey, N. de Cacqueray, C. Bailly, A shock-capturing methodology based on adaptative spatial filtering for high-order non-linear computations, J. Comp. Phys. 228 (2009) 1447–1465.

[31] S. Laizet, E. Lamballais, High-order compact schemes for incompressible flows: a simple and efficient method with quasi-spectral accuracy, J. Comp. Phys. 228 (2009) 5989–6015.

[32] R. Peyret, Introduction to high-order approximation methods for computational fluid dynamics, in: E. K. R. Peyret (Ed.), Advanced Turbulent Flow Computations, Springer, Vienna, 2000, pp. 1–79.

[33] R. S. Rogallo, An illiac program for the numerical simulation of homogeneous, incompressible turbulence, Tech. rep., NASA TM-73203 (1977).

[34] C. Canuto, M. Y. Hussaini, A. Quarteroni, T. A. Zang, Spectral Methods in Fluid Dynamics, Springer-Verlag, New York, 1988.

[35] S. Laizet, E. Lamballais, J. C. Vassilicos, A numerical strategy to combine high-order schemes, complex geometry and parallel computing for high resolution DNS of fractal generated turbulence, Computers and Fluids 39 (3) (2010) 471–484.

[36] S. Laizet, N. Li, Incompact3d: a powerful tool to tackle turbulence problems with up to $O(10^5)$ computational cores, Int. J. Numer. Methods Fluids 67 (11) (2011) 1735–1757.

[37] P. Bartholomew, G. Deskos, R. Frantz, F. Schuch, E. Lamballais, S. Laizet, Xcompact3d: An open-source framework for solving turbulence problems on a Cartesian mesh, SoftwareX 12 (2020) 100550.

[38] E. Lamballais, T. Dairay, S. Laizet, C. Vassilicos, Implicit/explicit spectral viscosity and large-scale SGS effects, in: M. Salvetti, V. Armenio, J. Fröhlich, B. Geurts, H. Kuerten (Eds.), Direct and Large-Eddy Simulation XI, Vol. 25, ERCOFTAC Series, Springer, Cham, 2019, pp. 107–113.

[39] R. Gautier, S. Laizet, E. Lamballais, A DNS study of jet control with microjets using an immersed boundary method, Int. J. Comp. Fluid Dynamics 28 (6-10) (2014) 1–18.

[40] M. Piller, Direct numerical simulation of turbulent forced convection in a pipe., Int. J. Numer. Methods Fluids **49** (2005) 583–602.

[41] T. Dairay, E. Lamballais, S. Benhamadouche, Mesh node distribution in terms of wall distance for large-eddy simulation of wall-bounded flows, Flow Turb. Combust. 100 (3) (2018) 617–626.

[42] E. Lamballais, R. Vicente Cruz, From explicit to implicit subgrid-scale and wall modelling in large-eddy simulation, in: B. Skallerud, H. I. Andersson (Eds.), MekIT'19, Tenth national conference on Computational Mechanics, Trondheim, Norway, 2019, pp. 1–24.

[43] S. Straub, P. Forooghi, L. Marocco, T. Wetzel, R. Vinuesa, P. Schlatter, B. Frohnapfel, The influence of thermal boundary conditions on turbulent forced convection pipe flow at two Prandtl numbers, Int. J. Heat and Mass Transfer 144 (2019) 118601.

[44] R. Vicente Cruz, E. Lamballais, R. Perrin, Implicit wall-layer modelling in turbulent pipe flow, in: S. M. Garca-Villalba M., Kuerten H. (Ed.), Direct and Large Eddy Simulation XII, Vol. 27, ERCOFTAC Series, Springer, Cham, 2020, pp. 425–431.

[45] G. K. E. Khoury, P. Schlatter, A. Noorani, P. F. Fischer, G. Brethouwer, A. V. Johansson, Direct numerical simulation of turbulent pipe flow at moderately high Reynolds numbers, Flow Turb. Combust. 91 (3) (2013) 475–495.

[46] O. A. Mahfoze, S. Laizet, Non-explicit large eddy simulations of turbulent channel flows from $Re_\tau = 180$ up to $Re_\tau = 5,200$, Int. J. Numer. Methods Fluids submitted (2020) 1–46.

[47] J.-C. Vassilicos, Dissipation in turbulent flows, Ann. Rev. Fluid Mech. 47 (2014) 95–114.

[48] M. O. Deville, P. F. Fischer, E. H. Mund, High-order methods for incompressible fluid flow, Cambridge University press, 2002.

[49] G. Karniadakis, S. Sherwin, Spectral/hp Element Methods for Computational Fluid Dynamics, 2nd Edition, Oxford science publications, 2005.

[50] M. de la Llave Plata, E. Lamballais, F. Naddei, On the performance of a high-order multiscale DG approach to LES at increasing Reynolds number, Computers and Fluids 194 (2019) 104306.

[51] F. Navah, M. de la Llave Plata, V. Couaillier, A high-order multiscale approach to turbulence for compact nodal schemes, Comput. Methods Appl. Mech. Engrg. 363 (2020) 112885.